

One-Point Probability Distribution Functions of Supersonic Turbulent Flows in Self-Gravitating Media

Ralf S. Klessen

Sterrewacht Leiden, Postbus 9513, 2300-RA Leiden, The Netherlands
Max-Planck-Institut für Astrophysik, Königstuhl 17, 69117 Heidelberg, Germany

(accepted for publication in The Astrophysical Journal)

ABSTRACT

Turbulence is essential for understanding the structure and dynamics of molecular clouds and star-forming regions. There is a need for adequate tools to describe and characterize the properties of turbulent flows. One-point probability distribution functions (pdf's) of dynamical variables have been suggested as appropriate statistical measures and applied to several observed molecular clouds. However, the interpretation of these data requires comparison with numerical simulations. To address this issue, SPH simulations of driven and decaying, supersonic, turbulent flows with and without self-gravity are presented. In addition, random Gaussian velocity fields are analyzed to estimate the influence of variance effects. To characterize the flow properties, the pdf's of the density, of the line-of-sight velocity centroids, and of the line centroid increments are studied. This is supplemented by a discussion of the dispersion and the kurtosis of the increment pdf's, as well as the spatial distribution of velocity increments for small spatial lags. From the comparison between different models of interstellar turbulence, it follows that the inclusion of self-gravity leads to better agreement with the observed pdf's in molecular clouds. The increment pdf's for small spatial lags become exponential for all considered velocities. However, all the processes considered here lead to non-Gaussian signatures, differences are only gradual, and the analyzed pdf's are in addition projection dependent. It appears therefore very difficult to distinguish between different physical processes on the basis of pdf's only, which limits their applicability for adequately characterizing interstellar turbulence.

Subject headings: hydrodynamics — ISM: clouds — ISM: kinematics and dynamics — turbulence

1. Introduction

Turbulence is an important ingredient for understanding the properties and characteristics of molecular clouds and star-forming regions. Turbulent gas motions are highly supersonic as indicated by the superthermal line widths ubiquitously observed throughout molecular clouds (Williams, Blitz & McKee 2000). These motions carry enough energy to halt global collapse and act as stabilizing agent for the entire cloud. However, it can be shown that interstellar turbulence decays quite rapidly on time scales of the order of the free-fall time of the system (Mac Low et al. 1998, Stone, Ostriker & Gammie 1998, Padoan & Nordlund 1999). To explain the observed long life times, turbulence in molecular clouds must be constantly driven (Gammie & Ostriker 1996, Mac Low 1999). The interplay between self-gravity on the one hand (leading to local collapse and star formation) and turbulent gas motion on the other hand (trying to prevent this process) plays a key role in determining the structure of molecular clouds. Altogether, understanding the characteristics of compressible, supersonic, and constantly replenished turbulence in self-gravitating media is an important ingredient for an adequate description of molecular clouds dynamics. And vice versa, from analyzing the spatial and dynamical structure of molecular clouds we can gain insight into the phenomenon of turbulence (for an overview over interstellar turbulence see Franco & Carraminana 1999).

Unfortunately, a complete and comprehensive theory of turbulence does not exist. Due to the enormous complexity of the problem, progress has been slow since Kolmogorov's pioneering work in 1941, where he derived simple scaling laws for incompressible, stationary, and homogeneous turbulence by postulating a self-similar energy cascade downwards from the driving scale to the dissipation range. Most effort has since been put in finding an adequate closure procedure, i.e. in finding a way to express the highest-order correlation in the hierarchy of equations governing turbulent motion (for an excellent overview see Lesieur 1997; also Boratav, Eden & Erzan 1997). However, a satisfying description of turbulence has yet to be found.

Correlation and distribution functions of dynamical variables are frequently deployed for characterizing the kinematical properties of turbulent molecular clouds. Besides using 2-point statistics (e.g. Scalo 1984, Kleiner & Dickman 1987, Kitamura et al. 1993, Miesch & Bally 1994, LaRosa, Shore & Magnani 1999), many studies have hereby concentrated on 1-point statistics, namely on analyzing the probability distribution function (pdf) of the (column) density and of dynamical observables, e.g. of the centroid velocities of molecular lines and their increments. The density pdf has been used to characterize numerical simulations of the interstellar medium by Vázquez-Semadeni (1994), Padoan, Nordlund, & Jones (1997), Passot, & Vázquez-Semadeni (1998) and Scalo et al. (1998). Velocity

pdf’s for several star-forming molecular clouds have been determined by Miesch & Scalo (1995) and Miesch, Scalo & Bally (1998). Lis et al. (1996, 1998) analyzed snapshots of a numerical simulation of mildly supersonic, decaying turbulence (without self-gravity) by Porter, Pouquet, & Woodward (1994) and applied the method to observations of the ρ -Ophiuchus cloud. Altogether, the observed pdf’s exhibit strong non-Gaussian features, they are often nearly exponential with possible evidence for power-law tails in the outer parts. This disagrees with the nearly Gaussian behavior typically found in experimental measurements and numerical models of incompressible turbulence. The observed centroid velocity *increment* pdf’s are more strongly peaked and show stronger deviations from Gaussianity than numerical models of incompressible turbulence predict. Furthermore, the spatial distribution of the largest centroid velocity differences (determining the tail of the distribution) appears ‘spotty’ across the face of the clouds; there is no convincing evidence for filamentary structure. Miesch et al. (1998) conclude that turbulence in molecular clouds involves physical processes that are not adequately described by incompressible turbulence or mildly supersonic decay simulations (see also Mac Low & Ossenkopf 2000).

It is the principal goal of this paper to extend previous determinations of pdf’s from numerical models into a regime more applicable for interstellar turbulence by (1) by calculating fully supersonic flows, (2) by including self-gravity, and (3) by incorporating a (simple analytic) description of turbulent energy input. For comparison with molecular cloud observations, I discuss the dynamical properties of decaying and stationary (i.e. driven), supersonic, isotropic turbulence in self-gravitating isothermal gaseous media. The pdf’s for the density, for the line centroid velocity and for their increments are derived as function of time and evolutionary state of the turbulent model.

The structure of this paper is as follows: Section 2 introduces and defines the statistical tools applied in the current study. It is followed in Sec. 3 by a description of the numerical scheme used to compute the time evolution of the turbulent flows. Sec. 4 shows that already simple variance effects in random Gaussian fields are able to introduce strong *non*-Gaussian distortions to the pdf’s which makes a clear-cut interpretation difficult. Section 5 contains the analysis of decaying, initially highly supersonic turbulence without self-gravity. This effect is then added to the simulations presented in Sec. 6. The model most relevant for molecular cloud dynamics is discussed in Sec. 7. It includes a simple driving term to replenish the turbulent cascade. Finally, in Sec. 8 all results are summarized.

2. PDF’s and Their Interpretation

2.1. Turbulence and PDF's

The Kolmogorov (1941) approach to incompressible turbulence is a purely phenomenological one and assumes the existence of a stationary turbulent cascade. Energy is injected into the system at large scales and cascades down in a self-similar way. At the smallest scales it gets converted into heat by molecular viscosity. The flow at large scales is essentially inviscid, hence for small wave numbers the equation of motion is dominated by the advection term. If the stationary state of fully developed turbulence results from random external forcing then one naïvely expects the velocity distribution in the fluid to be Gaussian on time scales larger than the correlation time of the forcing, irrespectively of the statistics of the forcing term which follows from the central limit theorem. However, the situation is more complex (e.g. Frisch 1995, Lesieur 1997). One of the most striking (and least understood) features of turbulence is its intermittent spatial and temporal behavior. The structures that arise in a turbulent flow manifest themselves as high peaks at random places and at random times. This is reflected in the pdf's of dynamical variables or passively advected scalars. They are sensitive measures of deviations from Gaussian statistics. Rare strong fluctuations are responsible for extended tails, whereas the much larger regions of low intensity contribute to the peak of the pdf near zero (for an analytical approach see e.g. Forster, Nelson & Stephens 1977, Falkovich & Lebedev 1997, Chertkov, Kolokolov & Vergassola 1997, Balkovsky et al. 1997, Balkovsky & Falkovich 1998). For incompressible turbulence the theory predicts velocity pdf's which are mainly Gaussian with only minor enhancement at the far ends of the tails. The distribution of velocity *differences* (between locations in the system separated by a given shift vector $\Delta\vec{r}$) is expected to deviate considerably from being normal and is likely to resemble an exponential. This finding is supported by a variety of experimental and numerical determinations (e.g. Kida & Murakami 1989, Vincent & Meneguzzi 1991, Jayesh & Warhaft 1991, She 1991, She, Jackson & Orszag 1991, Cao, Chen, & She 1996, Vainshtein 1997, Lamballais, Lesieur, & Métais 1997, Machiels & Deville 1998). Compressible turbulence has remained to be too complex for a satisfying mathematical analysis.

2.2. PDF's of Observable Quantities

It is not clear how to relate the analytical work on incompressible turbulence to molecular clouds. In addition to the fact that interstellar turbulence is highly supersonic and self-gravitating, there are also observational limitations. Unlike the analytical approach or numerical simulations, molecular cloud observations allow access only to dimensionally reduced information. Velocity measurements are possible only along the line-of-sight, and

the spatial structure of a cloud is only seen in projection onto the plane of the sky, i.e. as variations of the column density. Although some methods can yield information about the 3-dimensional spatial structure of the cloud (see Stutzki & Güsten 1990, Williams, De Geus, & Blitz 1994), the result is always model dependent and equivocal (see also Ballesteros-Paredes, Vázquez-Semadeni, & Scalo 1999).

A common way of obtaining knowledge about the velocity structure of molecular clouds is to study individual line profiles at a large number of various positions across the cloud. In the optical thin case line shapes are in fact histograms of the radial velocities of gas sampled along the telescope beam. Falgarone & Phillips (1990) and Falgarone et al. (1994) showed that line profiles constructed from high-sensitivity CO maps exhibit non-Gaussian wings and attributed this to turbulent intermittency (see also Falgarone et al. 1998 on results from the IRAM-key project). Dubinski, Narayan, & Phillips (1995) demonstrated that non-Gaussian line profiles can be produced from *any* Gaussian random velocity field if variance effects become important (which is always the case for very steep or truncated power spectra). They concluded that non-Gaussian line profiles do not provide clear evidence for intermittency.

Another method of inferring properties of the velocity distribution in molecular clouds is to analyze the pdf of line centroid velocities obtained from a large number of individual measurements scanning the entire projected surface area of a cloud (Miesch & Scalo 1995, Lis et al. 1998, Miesch et al. 1998). Each line profile (i.e. the pdf *along* the line-of-sight) is collapsed into one single number, the centroid velocity, and then sampled *perpendicular* to the line-of-sight. Hence, the two functions differ in the direction of the sampling and in the quantity that is considered. A related statistical measure is the pdf of centroid velocity increments, it samples the velocity differences between the centroids for line measurements which are offset by a given separation. The observational advantage of using centroid and increment pdf's is, that the line measurements can typically be taken with lower sensitivity as only the centroid has to be determined instead of the detailed line shape. These measures are also less dependent on large-scale systematic motions of the cloud and they are less effected by line broadening due to the possible presence of warm dilute gas. However, to allow for a meaningful analysis of the pdf's especially in the tails, the number of measurements needs to be very large and should not be less than about 1000. In order to sample the entire volume of interstellar clouds, the molecular lines used to obtain the pdf's are optically thin. I follow this approach in the present investigation and use a mass-weighted velocity sampling along the line-of-sight to determine the line centroid. This zero-opacity approximation does not require any explicit treatment of the radiation transfer process.

The observed pdf’s are obtained from *averaged* quantities (from column densities or line centroids). To relate these observational measures to quantities relevant for turbulence theory, i.e. to the full 3-dimensional pdf, numerical simulations are necessary as only they allow unlimited access to all variables in phase space. A first attempt to do this was presented by Lis et al. (1996, 1998) who analyzed a simulation of mildly supersonic decaying hydrodynamic turbulence by Porter et al. (1994). Since their model did neither include self-gravity nor consider flows at high Mach number or mechanisms to replenish turbulence, the applicability to the interstellar medium remained limited. This fact prompts the current investigation which extends the previous ones by calculating *highly supersonic flows*, and by including *self-gravity* and a *turbulent driving scheme*. The current study does not consider magnetic fields. Their influence on the pdf’s needs to be addressed separately. However, the overall importance of magnetic fields and MHD waves on the dynamical structure of molecular clouds may not be large. The energy associated with the observed fields is of the order of the (turbulent) kinetic energy content of molecular clouds (Crutcher 1999). Magnetic fields cannot prevent the decay of turbulence (e.g. Mac Low et al. 1998) which implies the presence of external driving mechanisms. These energy sources replenish the turbulent cascade and may excite MHD waves explaining the inferred equipartition between turbulent and magnetic energies.

2.3. Statistical Definitions

The one-point probability distribution function $f(x)$ of a variable x is defined such that $f(x)dx$ measures the probability for the variable to be found in the interval $[x, x + dx]$. The *density pdf* (ρ -pdf) discussed in this paper is obtained from the local density associated with each SPH particle. It is basically the normalized histogram summed over all particles in the simulation, i.e. a mass-weighted sampling procedure is applied. The *line-of-sight velocity centroid pdf* (v -pdf) is more complicated to compute. The face of the simulated cube is divided into 64^2 equal-sized cells. For each cell, the line profile is computed by sampling the normal (line-of-sight) velocity component of all gas particles that are projected into that cell. The line centroid is determined as the abscissa value of the peak of the distribution. This procedure corresponds to the formation of optically thin lines in molecular clouds, where all molecules within a certain column through the clouds contribute equally to the shape and intensity of the line. To reduce the sampling uncertainties, this procedure is repeated with the location of the cells shifted by half a cell size in each direction. Altogether about 20 000 lines contribute to the pdf. This is procedure is repeated for line-of-sights along all three system axes to identify projection effects. The *line centroid increment pdf* (Δv -pdf) is obtained in a similar fashion. However, the sampled quantity is now the velocity

difference between line centroids obtained at two distinct locations separated across the face of the cloud by a fixed shift vector $\Delta\vec{r}$. The Δv -pdf for a spatial lag Δr is obtained as azimuthal average, i.e. as superposition of all individual pdf's with shift vectors of length Δr .

Also statistical moments of the distribution can be used to quantify the spread and shape of pdf's. For the current analysis I use the first four moments. Mean value μ and standard deviation σ (the 1. and 2. moments) quantify the location and the width of the pdf and are given in units of the measured quantity. The third and fourth moments, skewness θ and kurtosis κ , are dimensionless quantities characterizing the shape of the distribution. The skewness θ describes the degree of asymmetry of a distribution around its mean. The kurtosis κ measures the relative peakedness or flatness of the distribution. I use a definition where $\kappa = 3$ corresponds to a normal distribution. Smaller values indicate existence of a flat peak compared to a Gaussian, larger values point towards a stronger peak or equivalently towards the existence of prominent tails in the distribution. A pure exponential results in $\kappa = 6$. Gaussian random fields are statistically fully determined by their mean value and the 2-point correlation function, i.e. by their first two moments, μ and σ . All higher moments can be derived from those. The 2-point correlation function is equivalent to the power spectrum in Fourier space (e.g. Bronstein & Semendjajew 1979).

Besides using moments there are other possibilities of characterizing a distribution. Van den Marel & Franx (1993) and Dubinski et al. (1995) applied Gauss-Hermite expansion series to quantify non-normal contributions in line profiles. A more general approach has been suggested by Vio et al. (1994), who discuss alternatives to the histogram representation of pdf's. However, as astrophysical data sets typically *are* histograms of various types and as histograms are the most commonly used method to describe pdf's, this approach is also adopted here.

3. The Numerical Model

3.1. SPH in Combination with GRAPE

SPH (*smoothed particle hydrodynamics*) is a particle-based scheme to solve the equations of hydrodynamics. The fluid is represented by an ensemble of particles, each carrying mass, momentum, and hydrodynamic properties. The time evolution of the fluid is represented by the time evolution of the particles, governed by the equations of motion which are supplemented by a prescription to modify the hydrodynamic properties. At any location these properties are obtained by averaging over an appropriate set of neighboring

particles. Excellent overviews over the method provide the reviews by Benz (1990) and Monaghan (1992). For the current study I use SPH because it is intrinsically Lagrangian and because it is able to resolve very high density contrasts. Another reason for choosing SPH is the possibility to use it in combination with the special-purpose hardware device GRAPE (Sugimoto et al. 1990, Ebisuzaki et al. 1993; and also Umemura et al. 1993, Steinmetz 1996). This allows calculations at supercomputer level on a normal workstation.

The code is based on a version originally developed by Benz (1990), and is used with a standard description of a von Neumann-type artificial viscosity (Monaghan & Gingold 1983) with the parameters $\alpha_v = 1$ and $\beta_v = 2$ for the linear and quadratic terms. The system is subject to periodic boundary conditions (Klessen 1997) and is integrated in time using a second-order Runge-Kutta-Fehlberg scheme, allowing individual time steps for each particle. Furthermore, the smoothing volume over which hydrodynamic quantities are averaged in the code is freely adjustable in space and time such that the number of neighbors for each particle remains approximately fifty. When including self-gravity, regions with masses exceeding the Jeans limit become unstable and collapse. Once a highly-condensed core has formed in the center of a collapsing gas clump, that core is substituted by a ‘sink’ particle (Bate, Bonnell, & Price 1995) which inherits the combined masses, linear and ‘spin’ angular momenta of the particles it replaces. It also has the ability to accrete further SPH particles from its infalling gaseous envelope.

For simulations of turbulent flows one also has to take into account that an explicit viscosity term is introduced in the SPH method. This fact demands attention when studying dissipative processes, especially in the subsonic regime. The current study focuses on the properties of highly supersonic turbulent flows. In this regime, direct comparison between SPH and grid-based methods has proven the close correspondence of both methods (Mac Low et al. 1998, Klessen, Heitsch & Mac Low 2000). If one bears the above caveats in mind, the SPH method calculates the time evolution of gaseous systems very reliably and accurately, and offers large spatial and dynamical flexibility.

3.2. Models

The numerical models discussed here describe isothermal gas. The hydrodynamic equations are extended to include self-gravity (in Sec.’s 6 and 7) and to incorporate a random turbulent driving mechanism (in Sec. 7). All physical constants are set to unity. The same applies to mass and length scales, i.e. the total mass is $M = 1$ and the simulated volume is the cube $[-1, +1]^3$. The mean density is thus $\rho = 1/8$. The initial configuration of all dynamical systems discussed in this paper is a homogeneous gas distribution with a

Gaussian velocity field. Without turbulence, the time evolution depends on one parameter, the *ratio* between internal and gravitational energy, $\alpha \equiv \epsilon_{\text{int}}/|\epsilon_{\text{pot}}|$. This quantity can be interpreted as dimensionless temperature and determines the number of thermal Jeans masses contained in the system. Molecular clouds are characterized by line widths which largely exceed the thermal broadening. The evolution away from the homogeneous initial state is thus strongly influenced by the adopted initial velocity distribution and depends on whether turbulence is decaying or driven. Large turbulent kinetic energy can considerably slow down or even prevent the collapse of thermally Jeans unstable gas. The situation is very complex and depends on the shape and strength of the turbulent velocity spectrum (Klessen et al. 2000; see also see Bonazzola et al. 1992 and Vázquez-Semadeni & Gazol 1995 for an analytical approach).

To generate and maintain turbulent flows Gaussian velocity fields are introduced. The spatial variations of each component of the velocity vector \vec{v} are described as superpositions of plane waves with wave numbers $\vec{k} = (k_x, k_y, k_z)$, where the phase of each wave is random and sampled from a uniform distribution in the interval $[0, 2\pi[$. Also the amplitude is random, but selected from a Gaussian distribution centered on zero and with a width determined by the power spectrum $P(k) = A_k k^\alpha$. Gaussian fields are isotropic and only depend on the absolute value of the wave vector $k = |\vec{k}|$. Only waves in the range $1 \leq k \leq k_{\text{max}}$ are considered. For large cut-off wave numbers k_{max} the Gaussian statistics is very well sampled. If only very few modes are used to generate the field, variance effects become strong and individual realizations of the field can deviate significantly from the ensemble average (see Sec. 4). The field is then transformed back into real space and the resulting velocities are assigned to individual SPH particles using the ‘cloud-in-cell’ scheme (Hockney & Eastwood 1988). For the initial field, all velocities are multiplied by the appropriate factor to reach the desired rms Mach number of the flow. In case of driven turbulence, this velocity field is also used to ‘kick’ the SPH particles at every time step such that a constant level of kinetic energy is maintained (see Mac Low 1999)

4. PDF’s from Gaussian Velocity Fluctuations

Variance effects in poorly sampled Gaussian velocity fields can lead to considerable *non-normal* contributions to the v - and Δv -pdf’s. If a random process is the result of sequence of independent events (or variables), then in the limit of large numbers, its distribution function will be a Gaussian around some mean value. However, only the properties of a large *ensemble* of Gaussian fields are determined in a statistical sense. Individual realizations may exhibit considerable deviations from the mean. The effect is

strongest when only few (spatial) modes contribute to the field or, almost equivalently, when the power spectrum falls off very steeply. In this case, most kinetic energy is in large-scale motions.

This is visualized in Fig. 1, it shows v -pdf's for homogeneous gas (sampled by 64^3 SPH particles placed on a regular grid) with Gaussian velocity fields with power spectra $P(k) = \text{const.}$ which are truncated at different wave numbers k_{max} ranging from (a) $k_{\text{max}} = 2$ to (d) $k_{\text{max}} = 32$. Each realization is scaled such that the rms velocity dispersion is $\sigma_v = 0.5$. The figure displays the pdf's for the x -, y -, and z -component of the velocity. The pdf's of the strongly truncated spectrum (Fig. 1a) do not at all resemble normal distributions. The Gaussian statistics of the field is very badly sampled with only very few modes. Note that the pdf's of the same field may vary considerably for different velocity *components*, i.e. for different *projections*. With the inclusion of larger number of Fourier modes this situation improves, and in Fig. 1d the pdf's of all projections sample the expected Gaussian distribution very well.

A similar conclusion can be derived for Δv -pdf. This measure is even more sensitive to deviations from Gaussian statistics. Figure 2 plots the Δv -pdf's for the same sequence of velocity fields. For brevity, only the line-of-sight component parallel to the x -axis is considered. Furthermore, from the sequence of possible Δv -pdf's (defined by the spatial lag Δr) only three are shown, at small ($\Delta r = 1/32$, upper curve), medium ($\Delta r = 10/32$, middle curve), and large spatial lags ($\Delta r = 30/32$, lower curve). Sampling the Gaussian field with only two modes (Fig. 2a) is again insufficient to yield increment pdf's of normal shape. The velocity field is very smooth, and the line centroid velocity difference between neighboring cells is very small. Hence, for $\Delta r = 1/32$ the pdf is dominated by a distinct central peak at $\Delta v = 0$. The tails of the distribution are quite irregularly shaped. The situation becomes 'better' when sampling increasing distances, as regions of the fluid separated by larger Δr are less strongly correlated in velocity. For $\Delta r = 10/32$ and $\Delta r = 30/32$ the pdf's follow the Gaussian distribution more closely although irregularities in the shapes are still present. In Fig.'s 2b and c the Δv -pdf's for medium to large lags are very well fit by Gaussians. Deviations occur only at small Δr , the pdf's are exponential (and the distribution for $k_{\text{max}} = 4$ is still a bit cuspy). Finally, Fig. 2d shows the three Δv -pdf's for the case where all available spatial modes contribute to the velocity field ($1 \leq k \leq 32$). The pdf's follow a Gaussian for all spatial lags.

This behavior is also seen in the variation of the moments of the distribution as function of the spatial lag Δr . Applied to the above sequence of Gaussian velocity fields, Fig. 3 displays the dispersion σ and the kurtosis κ of the distribution. The corresponding models are indicated at the right hand side of each plot. The width of the distribution,

as indicated by the dispersion σ (Fig. 3a), typically grows with increasing Δr , reflecting the relative peakedness of the distribution at small lags. For example, the distribution (a) yields a slope of 0.3 in the range $-0.6 \leq \log_{10} \Delta r \leq -0.4$, and (b) leads to a value of 0.2 in relatively large interval $-1.5 \leq \log_{10} \Delta r \leq -0.5$. The effect disappears for the better sampled fields. Typical values for that slope in observed molecular clouds are -0.3 to -0.5 (Miesch et al. 1998).¹ A direct measure of the peakedness of the distribution is its fourth moment, the kurtosis κ (Fig. 3b). At small lags Δr , clearly the pdf's of model (a) are more strongly peaked than exponential ($\kappa = 6$). Comparing the entire sequence reveals again the tendency of the pdf's to become Gaussian at decreasing Δr with increasing number of modes considered in the construction of the velocity field.

Taking all together, it is advisable to consider conclusions about interstellar turbulence derived from solely analyzing one-point probability distribution functions from molecular clouds with caution. Similar to what has been shown by Dubinski et al. (1995) for molecular line profiles, deviations from the regular Gaussian shape found in v - and Δv -pdf's need not be the signpost of turbulent intermittency. Gaussian velocity fields which are dominated by only a small number of modes (either because the power spectrum falls off steeply towards larger wave numbers, or because small wave length distortions are cut away completely) will lead to very similar distortions. In addition, the properties of the pdf may vary considerably between different projections. The same velocity field may lead to smooth and Gaussian pdf's for one velocity component, whereas another projection may result in strong non-Gaussian wings (see also Fig. 9).

5. Analysis of Decaying Supersonic Turbulence without Self-Gravity

In this section the pdf's of freely decaying initially highly supersonic turbulence without self-gravity are discussed. They are calculated from an SPH simulation with 350 000 particles (Mac Low et al. 1998, model G). Initially the system is homogeneous with a Gaussian velocity distribution with $P(k) = \text{const.}$ in the interval $1 \leq k \leq 8$. The rms Mach number of the flow is $M = 5$.

¹Note, that Miesch et al. (1998) are plotting the function σ^2 versus the spatial lag Δr . For a comparison with the present study, their numbers have to be divided by a factor of two. Furthermore, they use a relatively narrow range of Δr -values to compute the slope of the function; larger intervals would on average tend to decrease these values (see their Fig. 14). In addition, Miesch et al. (1998) applied spatial filtering to remove large-scale velocity gradients in the clouds. These would lead to steeper slopes. The fact that in the present study the functions σ and κ level out for large spatial lags Δr is a consequence of the periodic boundary conditions which do not allow for large-scale gradients.

After the onset of the hydrodynamic evolution the flow quickly becomes fully turbulent resulting in rapid dissipation of kinetic energy. The energy decay is found to follow a power law $t^{-\eta}$ with exponent $\eta = 1.1 \pm 0.004$. The overall evolution can be subdivided into several phases. The first phase is very short and is defined by the transition of the initially Gaussian velocity field into fully developed supersonic turbulence. It is determined by the formation of the first shocks which begin to interact with each other and build up a complex network of intersecting shock fronts. Energy gets transferred from large to small scales and the turbulent cascade builds up. The second phase is given by the subsequent self-similar evolution of the network of shocks. Even though individual features are transient, the overall properties of this network change only slowly. In this phase of highly supersonic turbulence the loss of kinetic energy is dominated by dissipation in shocked regions. In the transsonic regime, i.e. the transition from highly supersonic to fully subsonic flow, energy dissipation in vortices generated by shock interactions becomes more and more important. Only the strongest shocks remain in this phase. Surprisingly, the energy decay law does not change during this transition. It continues to follow a power law with exponent $\eta \approx 1$. In the subsonic phase the flow closely resembles incompressible turbulence. Its properties are similar to those reported from numerous experiments and simulations (e.g. Porter et al. 1994, Lesieur 1997, Boratav et al. 1997). The simulation is stopped at $t = 20.0$ when the flow has decayed to a rms Mach number of $M = 0.3$. Since the energy loss rate follows a power law, the duration of each successive phase grows.

This sequence of evolutionary stages is seen in the pdf's of the system. One noticeable effect is the decreasing width of the distribution functions as time progresses. As the kinetic energy decays the available range of velocities shrinks. This not only leads to 'smaller' v - and Δv -pdf's, but also to a smaller ρ -pdf since compressible motions lose influence and the system becomes more homogeneous. This is indicated in Fig. 4, it displays (a) the ρ -pdf and (b) v -pdf at the following stages of the dynamical evolution (from top to bottom): Shortly after the start, at $t = 0.2$ when the first shocks occur, then at $t = 0.6$ when the network of interacting shocks is established and supersonic turbulence is fully developed, during the transsonic transition at $t = 3.5$, and finally at $t = 20.0$ when the flow has progressed into the subsonic regime. The rms Mach numbers at these stages are $M = 5.0$, $M = 2.5$, $M = 1.0$, and $M = 0.3$, respectively. The density pdf always closely follows a log-normal distribution, i.e. it is Gaussian in the *logarithm* of the density. Also the distribution of line centroids at the four different evolutionary stages of the system is best described by a Gaussian with only minor deviations at the far ends of the velocity spectrum.

For the same points in time, Fig. 5 shows the Δv -pdf's for x -component of the velocity. The displayed spatial lags are selected in analogy to Fig. 2. Note the different velocity

scaling in each plot reflecting the decay of turbulent energy as the system evolves in time. Throughout the entire sequence, spatial lags larger than about 10% of the system size always lead to Δv -pdf's very close to Gaussian shape (the middle and lower curves). Considerable deviations occur only at small spatial lags (the upper curves). For those, the increment pdf's exhibit exponential wings during all stages of the evolution. When scaling the pdf's to the same width, the distribution in the subsonic regime (d) appears to be more strongly peaked than during the supersonic or transsonic phase (a – c). There, the central parts of the pdf's are still reasonably well described by the Gaussian obtained from the first two moments, whereas in (d) the peak is considerably narrower, or vice versa, the tails of the distribution are more pronounced.

These results can be compared with the findings by Lis et al. (1998). They report increment pdf's for three snapshots of a high-resolution hydrodynamic simulation of decaying mildly super-sonic turbulence performed by Porter et al. (1994). They analyze the system at three different times corresponding to rms Mach numbers of $M \approx 0.96$, $M \approx 0.88$, and $M \approx 0.52$. Their first two data sets thus trace the transition from supersonic to subsonic flow and are comparable to phase (c) of the current model; their last data set corresponds to to phase (d). In the transsonic regime both studies agree: Lis et al. (1998) report enhanced tails in the increment pdf's for the smallest spatial lags which they considered and near Gaussian distributions for larger lags (however, the largest separation they study is about 6% of the linear extent of the system). In the subsonic regime, Lis et al. (1998) find near Gaussian pdf's for very small spatial lags ($< 1\%$), but extended wings in the pdf's for lags of 3% and 6% of the system size. They associate this with the 'disappearance' of large-scale structure. Indeed, their Fig. 7 exhibits a high degree of fluctuations on small scales which they argue become averaged away when considering small spatial lags in the Δv -pdf. Comparing the pdf with spatial lags of 3% (upper curves in Fig. 5, compared to the pdf's labeled with $\Delta = 15$ in Lis et al. 1998) both studies come to the same result. At these scales the Δv -pdf's tend to exhibit more pronounced wings in the subsonic regime as in the supersonic regime. The SPH calculations reported here do not allow for a meaningful construction of δv -pdf's for $\Delta r < 3\%$. The Gaussian behavior of pdf's for very small spatial lags reported by Lis et al. (1998) therefore cannot be examined. However, neither of the purely hydrodynamic simulations lead to pdf's that are in good agreement with the observations. Observed pdf's typically are much more centrally peaked at small spatial separation (see e.g. Fig. 4 in Lis et al 1998 and Miesch et al. 1998).

Figure 6 shows the spatial distribution of centroid velocity differences between cells separated by a vector lag of $\Delta \vec{r} = (1/32, 1/32)$ (i.e. between neighboring cells along the diagonal). Data are obtained at the same times as above. Each figure displays the array of the absolute values of the velocity increments Δv_x in linear scaling as indicated at the

top. Note the decreasing velocity range reflecting the decay of turbulent energy. The distribution of Δv_x appears random, there is no clear indication for coherent structures. This corresponds to most observations. Miesch et al. (1998) find for their sample of molecular clouds that high-amplitude velocity differences for very small spatial lags typically are well distributed resulting in a ‘spotty’ appearance. Note, however, that using azimuthal averaging Lis et al. 1998 report the finding of filamentary structures for the ρ -Ophiuchus cloud. Altogether, filamentary structure is difficult to define and a mathematical thorough analysis is seldomly performed (for an astrophysical approach see Adams & Wiseman 1994, for a discussion of the filamentary vortex structure in incompressible turbulence consult Frisch 1995 or Lesieur 1997). The visual inspection of maps is often misleading and influenced by the parameters used to display the image. Larger velocity bins for instance tend to produce a more ‘filamentary’ structure than very fine sampling of the velocity structure. Further uncertainty may be introduced by the fact that molecular clouds are only seen in one projection as the signatures of the dynamical state of the system can strongly depend on the viewing angle.

6. Analysis of Decaying Turbulence with Self-Gravity

In this section, I discuss the properties of decaying, initially supersonic turbulence in a self-gravitating medium. Figure 7 displays an SPH simulation with 200 000 particles at six different times of its dynamical evolution. Since the model is subject to periodic boundary conditions, every figure has to be considered infinitely replicated in each direction. Analog to the previous model, the system is initially homogeneous and its velocity field is generated with $P(k) = \text{const.}$ using modes with wave numbers $1 \leq k \leq 8$. From the choice $\alpha = 0.01$ it follows that the system contains 120 *thermal* Jeans masses. The initial rms velocity dispersion is $\sigma_v = 0.5$ and with the sound speed $c_s = 0.082$ the rms Mach number follows as $M = 6$. These values imply that the initial turbulent velocity field contains sufficient energy to globally *stabilize* the system against gravitational collapse. Scaled to physical units using a density $n(\text{H}_2) = 10^5 \text{ cm}^{-3}$, which is typical for massively star-forming regions (e.g. Williams et al. 2000), the system corresponds to a volume of $[0.32 \text{ pc}]^3$ and contains a gas mass of $200 M_\odot$. As the simulation starts, the system quickly becomes fully turbulent and loses kinetic energy. Like in the case without self-gravity a network of intersecting shocks develops leading to density fluctuations on all scales. If the mass of a fluctuation exceeds the (local) Jeans limit it begins to contract due to self-gravity. During the early evolution, there is enough kinetic energy to prevent this collapse process on all scales (Fig. 7b – $t = 0.5$) and the properties of the system are similar to those of pure hydrodynamic turbulence. However, as time progresses and turbulent energy decays the effective Jeans

mass decreases. *Local* collapse of shock generated density fluctuations sets in despite the fact that the system is still globally stabilized by turbulence (see also Klessen et al. 2000). The central high-density cores of collapsing clumps are indicated by black dots. The cores form mainly at the intersection of filaments, where the density is highest and local collapse is most likely to set in. When turbulence is decayed sufficiently also large-scale collapse becomes possible. Gas clumps follow the global flow pattern towards a common center of gravity where they may merge or sub-fragment. Gradually a cluster of dense cores is built up. In the isothermal model this process continues until all available gas is accreted onto the ‘protostellar’ cluster (for more details Klessen & Burkert 2000).

The pdf’s of (a) the density and of (b) the x -component of the line centroid velocities for the above six model snapshots are displayed in Fig. 8. The corresponding time is indicated by the letters at the right side of each panel. During the dynamical evolution of the system the density distribution develops a high density tail. This is the imprint of local collapse. The densities of compact cores are indicated by solid dots (at $t = 2.0$ and $t = 2.5$). Virtually all particles in the high density tails at earlier times (at $t = 1.0$ and more so at $t = 1.5$) are accreted onto these cores. The bulk of matter roughly follows a log-normal density distribution as indicated by the dotted parabola. The v -pdf’s are nearly Gaussian as long as the dynamical state of the system is dominated by turbulence. Also the width of the pdf remains roughly constant during this phase. This implies that the decay of turbulent kinetic energy is in balance with the gain of kinetic energy due to gravitational (‘quasi-static’) contraction on large scales. The time scale for this process is determined by the energy dissipation in shocks and turbulent eddies. However, once *localized* collapse is able to set in, accelerations on small scales increase dramatically and the evolution ‘speeds up’. For times $t > 2.0$ the centroid pdf’s become wider and exhibit significant deviations from the original Gaussian shape. The properties of the pdf’s are similar to those observed in star-forming regions (Miesch & Scalo 1995, Lis et al. 1998, Miesch et al. 1998). This is expected since gravitational collapse is a necessary ingredient for forming stars.

Gravity creates *non*-isotropic density and velocity structure structures. When analyzing v - and Δv -pdf’s, their appearance and properties will strongly depend on the viewing angle. This is a serious point of caution when interpreting observational data, as molecular cloud are seen only in *one* projection. As illustration, Fig. 9 plots the centroid pdf at the time $t = 2.0$ for the line-of-sight projection along all three axes of the system. Whereas the pdf’s for the x - and the y -component of the velocity centroid are highly structured (upper and middle curve – the latter one is even double peaked), the distribution of the z -component (lowest curve) is smooth and much smaller in width, comparable to the ‘average’ pdf at *earlier* stages of the evolution. As the variations between different viewing angles or equivalently different velocity components can be very large, statements about

the 3-dimensional velocity structure from only observing one projection can be misleading.

Gravity effects the Δv -pdf. Figure 10 displays the increment pdf's at small, intermediate and large spatial lags, analog to Fig.'s 2 and 5. Time ranges from (a) $t = 1.0$ to (d) $t = 2.5$ corresponding to Fig.'s 7c–f. The pdf's for $t = 0.0$ and $t = 0.5$ are not shown since at these stages supersonic turbulence dominates the dynamic of the system and the pdf's are comparable to the ones without gravity (Fig. 5). This still holds for $t = 1.0$. The increment pdf's for medium to large spatial lags appear Gaussian, however, the pdf for the smallest lag follows a perfect exponential all the way inwards to $\Delta v = 0$. Unlike in the case without gravity, the peak of the distribution is not ‘round’, i.e. is not Gaussian in the innermost parts (when scaled to the same width). *It is a sign of self-gravitating systems that the increment pdf at smallest lags is very strongly peaked and remains exponential over the entire range of measured velocity increments.* This behavior is also seen Fig.'s 10b–d. At these later stages of the evolution in addition non-Gaussian behavior is also found at medium lags. This results from the existence of large-scale filaments and streaming motions. The same behavior is found for the increment pdf's from observed molecular clouds (for ρ -Ophiuchus see Lis et al 1998; for Orion, Mon R2, L1228, L1551, and HH83 see Miesch et al. 1998). In each case, the distribution for the smallest lag (one pixel size) is very strongly peaked at $\Delta v = 0$, in some cases even more than exponential. The deviations from the Gaussian shape remain for larger lags but are not so pronounced. The inclusion of self-gravity into models of interstellar turbulence leads to good agreement with the observed increment pdf's. However, this result may *not* be unique as in molecular clouds additional processes are likely to be present that could also lead to strong deviations from Gaussianity.

The time evolution of the statistical moments of the Δv -pdf's for various spatial lags is presented in Fig. 11. It plots (a) the dispersion σ , and (b) the kurtosis κ . The letters on the right-hand side indicate the corresponding time in Fig. 7. At $t = 0.0$ the width σ of the pdf is approximately constant for all Δr and the kurtosis κ is close to normal value of three. Both indicate that Gaussian statistics very well describes the initial velocity field. As turbulent energy decays, gravitational collapse sets in. Because of the gravitational acceleration, the amplitudes of centroid velocity differences between separate regions in the cloud grow larger, the width σ of the Δv -pdf's increases. This becomes more important when sampling velocity differences on larger spatial scales, hence σ also increases with Δr . The slope is $d \log_{10} \sigma / d \log_{10} \Delta r \lesssim 0.2$. For $\log_{10} \Delta r > -0.4$ it levels out, which is a result of the adopted periodic boundary conditions. They do not allow for large-scale velocity gradients. The increasing ‘peakedness’ of Δv -pdf is reflected in the large values of the kurtosis κ at the later stages of the evolution. For small spatial lags the pdf's are more centrally concentrated than exponential (i.e. $\kappa > 6$), and even at large spatial separations they are still more strongly peaked than Gaussian ($\kappa > 3$). The slope at $t = 2.5$

is $d \log_{10} \kappa / d \log_{10} \Delta r \approx -0.4$ which is indeed comparable to what is found in observed star-forming regions (Miesch et al. 1998).

For the above simulation of self-gravitating, decaying, supersonic turbulence, Fig.12 plots the 2-dimensional distribution of centroid increments for a vector lag $\Delta \vec{r} = (1/32, 1/32)$. The velocity profiles are sampled along the x -axis of the system. The magnitude of the velocity increment Δv_x is indicated at the top of each plot. The spatial distribution of velocity increments during the initial phases appears random. Later on, gravity gains influence over the flow and creates a network of intersecting filaments where gas streams onto and flows along towards local potential minima. At that stage, the velocity increments with the highest amplitudes tend to trace the large-scale filamentary structure. This is the sign of the anisotropic nature of gravitational collapse motions.

7. Analysis of Driven Turbulence with Self-Gravity

Figure 13 displays the gas distribution at different evolutionary stages of a simulation of driven, supersonic, self-gravitating turbulence. The number of SPH particles is 205 379. Again, the system is initially homogeneous in space and has a random Gaussian velocity field with flat power spectrum in the wave number interval $3 \leq k \leq 4$. It contains 64 *thermal* Jeans masses and turbulence is continuously driven as described in Sec. 3.2. The initial evolution into equilibrium between the energy input by the driving force and the decay of turbulent kinetic energy is computed without self-gravity, then it is turned on. This phase is displayed in Fig. 13a. In this state the *turbulent* Jeans mass (on scales larger than the maximum driving wave length) exceeds the total mass in the system by a factor of two, the cloud is therefore stabilized by turbulence against gravitational collapse on global scales. However, local collapse (on scales at or below the driving scale) is still possible and does occur. As in the previous case without driving, the dynamical evolution of the system leads to the formation of a cluster of dense collapsed cores. This is shown in Fig.'s 13b–d, which display the system when 20%, 40%, and 60% of the gas mass has accumulated in dense collapsed cores (at time $t = 1.8$, $t = 3.2$, and $t = 4.8$, respectively). However, in the presence of the driving source the time scales for accretion are longer and the cluster is less dense.

The pdf's of (a) the density and (b) the x -component of the line centroid velocities corresponding to the above four snapshots are displayed in Fig. 14. As in the previous model, the bulk of gas particles that are not accreted onto cores build up an approximately log-normal ρ -pdf (indicated by the dotted lines). Also the v -pdf remains close to the Gaussian value. This is different from the case of purely decaying self-gravitating turbulence,

where at some stage global collapse motions set in and lead to very wide and distorted centroid pdf's. This is not possible in the simulation of driven turbulence, as it is stabilized on the largest scales by turbulence. Collapse occurs only locally which leaves the width of the pdf's relatively unaffected and only mildly alters their shape.

Also the Δv -pdf's show no obvious sign of evolution. For the x -component of the velocity these functions are displayed in Fig. 15, again for three different spatial lags. The chosen times correspond (a) to the equilibrium state at $t = 0.0$, and (b) to $t = 4.8$ which is the final state of the simulation. The pdf's only marginally grow in width. At every evolutionary stage, the pdf for the smallest spatial lag is exponential, whereas the pdf's for medium and large shift vectors closely follow the Gaussian curve defined by the first two moments of the distribution (dotted lines). The functions are similar to the ones in the previous model before the large scale collapse motions set in (Fig. 10a, b). Only overall contraction will affect Δv -pdf at medium to large lags. This behavior also follows from comparing the statistical moments. Figure 16 plots (a) the dispersion σ and (b) the kurtosis κ as function of the spatial lag Δr . Figures 11a and 16a are very similar, as soon as turbulence is established the width σ of the pdf increases with Δr with a slope of $d \log_{10} \sigma / d \log_{10} \Delta r \lesssim 0.2$ for small to medium lags and levels out for larger ones. However, when comparing the 'peakedness' of the pdf as indicated by κ (Fig.'s 11b and 16b) the model of decaying self-gravitating turbulence yields much higher values since the pdf's are more strongly peaked due to the presence of large-scale collapse motions.

Figure 17 finally shows the spatial distribution of the x -component of the line centroid increments for a vector lag $\Delta \vec{r} = (1/32, 1/31)$. Since the increment maps at different evolutionary times are statistically indistinguishable, only times (a) $t = 0.0$ and (b) $t = 4.8$ are displayed in the figure. As in the case of supersonic, purely hydrodynamic turbulence the spatial distribution of velocity increments appears random and uncorrelated.

The adopted driving mechanism prevents global collapse. The bulk properties of the system therefore resemble hydrodynamic, *non*-self-gravitating turbulence. However, local collapse motions do exist and are responsible for noticeable distortions away from the Gaussian statistics. As the non-local driving scheme adopted here introduces a bias towards Gaussian velocity fields, these distortions are not very large. There is a need to introduce other, more realistic driving agents into this analysis. These could lead to much stronger non-Gaussian signatures in the pdf's.

8. Summary

SPH simulations of driven and decaying, supersonic, turbulent flows with and without self-gravity have been analyzed in this study . It extends previous investigations of mildly supersonic, decaying, *non*-self-gravitating turbulence (Lis et al. 1996, 1998) into a regime more relevant molecular clouds, by (a) considering highly supersonic flows and by including (b) self-gravity and (c) a driving source for turbulence.

The flow properties are characterized by using the probability distribution functions of the density, of the line-of-sight velocity centroids, and of their increments. Furthermore the dispersion and the kurtosis of the increment pdf's are discussed, as well as the spatial distribution of the velocity increments for the smallest spatial lags.

(1) To asses the influence of variance effects, simple Gaussian velocity fluctuations are studied. The insufficient sampling of random Gaussian ensembles leads to distorted pdf's similar to the observed ones. For line profiles this has been shown by Dubinski et al. (1995).

(2) Decaying, initially highly supersonic turbulence without self-gravity leads to pdf's which also exhibit deviations from Gaussianity. For the trans- and subsonic regime this has been reported by Lis et al. (1996, 1998). However, neglecting gravity and thus not allowing for the occurance of collapse motions, these distortions are not very pronounced and cannot account well for the observational data (Lis et al. 1998, Miesch et al. 1998).

(3) When including gravity into the models of decaying initially supersonic turbulence, the pdf's get into better agreement with the observations. During the early dynamical evolution of the system turbulence carries enough kinetic energy to prevent collapse on all scales. In this phase the properties of the system are similar to those of non-gravitating hydrodynamic supersonic turbulence. However, as turbulent energy decays gravitational collapse sets in. First localized and on small scales, but as the turbulent support continues to diminish collapse motions include increasingly larger spatial scales. The evolution leads to the formation of an embedded cluster of dense protostellar cores (see also Klessen & Burkert 2000). As the collapse scale grows, the ρ -, v -, and Δv -pdf's get increasingly distorted. In particular, the Δv -pdf's for small spatial lags are strongly peaked and exponential over the entire range of measured velocities. This is very similar to what is observed in molecular clouds (for ρ -Ophiuchus see Lis et al 1998; for Orion, Mon R2, L1228, L1551, and HH83 see Miesch et al. 1998).

(4) The most realistic model for interstellar turbulence considered here includes a simple (non-local) driving scheme. It is used to stabilize the system against collapse on large scales. Again non-Gaussian pdf's are observed. Despite global stability, local collapse is possible and the system again evolves towards the formation of an embedded cluster

of accreting protostellar cores. As the adopted driving scheme introduces a bias towards maintaining a Gaussian velocity distribution, the properties of the pdf's fall in between the ones of pure hydrodynamic supersonic turbulence and the ones observed in systems where self-gravity dominates after sufficient turbulent decay. This situation may change when considering more realistic driving schemes.

(5) A point of caution: The use of v - and Δv -pdf's to unambiguously characterize interstellar turbulence and to identify possible physical driving mechanisms may be limited. *All* models considered in the current analysis lead to non-Gaussian signatures in the pdf's, differences are only gradual. In molecular clouds the number of physical processes that are expected to give rise to deviations from Gaussian statistics is large. Simple statistical sampling effects (Sec. 4) and turbulent intermittency caused by vortex motion (Lis et al. 1996, 1998), as well as the effect self-gravity (Sec. 6) and of shock interaction in highly supersonic flows (Mac Low & Ossenkopf 2000), *all* will lead to non-Gaussian signatures in the observed pdf's. Also stellar feedback processes, galactic shear and the presence of magnetic fields will influence the interstellar medium and create distortions in the velocity field. This needs to be studied in further detail. In addition, the full 3-dimensional spatial and kinematical information is not accessible in molecular clouds, measured quantities are always projections along the line-of-sight. As the structure of molecular clouds is extremely complex, the properties of the pdf's may vary considerably with the viewing angle. Attempts to disentangle the different physical processes influencing interstellar turbulence therefore should not rely on analyzing velocity pdf's alone, they require additional statistical information.

I thank A. Burkert, F. Heitsch, and M.-M. Mac Low for many fruitful and stimulating discussions, and the editor S. Shore for his comments on the paper and his help with an extremely slow and non-responsive (anonymous) referee.

REFERENCES

- Adams, F.C., Wiseman, J.J. 1994, ApJ, 435, 693
Balkovsky, E., Falkovich, G. 1998, Phys. Rev. E, 57, R1231
Balkovsky, E., Falkovich, G., Kolokolov, I., Lebedev, V. 1997, Phys. Rev. Lett., 78, 1452
Ballesteros-Paredes, J., Vázquez-Semadeni, E., Scalo, J. 1999, ApJ, 515, 286
Bate, M.R., Bonnell, I.A., Price, N.M. 1995, MNRAS, 277, 362
Bate, M.R., Burkert, A. 1997, MNRAS, 288, 1060

- Benz, W. 1990, in *The Numerical Modeling of nonlinear Stellar Pulsations*, ed. J.R. Buchler, Kluwer Academic Publisher, Dordrecht
- Bonazzola, S., Perault, M., Puget, J.L, Heyvaerts, J., Falgarone, E., Panis, J.F. 1992, *J. Fluid. Mech.*, 245, 1
- Boratav, O., Eden, A., Erzan, A. (eds.) 1997, *Turbulence Modeling and Vortex Dynamics*, Springer Verlag, Heidelberg
- Bronstein, I.N., Semendjajew, K.A. 1979, *Taschenbuch der Mathematik*, Teubner Verlagsgesellschaft, Leipzig
- Burkert, A., Klessen, R.S., Bodenheimer, P. 1998, in *The Orion Complex Revisited*, eds. M. McCaughrean & A. Burkert, ASP Conference Series, in press
- Cao, N., Chen, S., She, Z.-S. 1996, *Phys. Rev. Lett.*, 76, 3711
- Chertkov, M., Kolokolov, I., Vergassola, M. 1997, *Phys. Rev. E*, 56, 5483
- Crutcher, R. M. 1999, *ApJ*, 520, 706
- Dubinski, J., Narayan, R., Phillips, T.G. 1995, *ApJ*, 448, 226
- Ebisuzaki, T., Makino, J., Fukushige, T., Taiji, M., Sugimoto, D., Ito, T., Okumura, S.K. 1993, *PASJ*, 45, 269
- Falgarone, E., Lis, D.C., Phillips, T.G., Pouquet, A., Porter, D.H., Woodward, P.R. 1994, *ApJ*, 436,728
- Falgarone, E., Panis, J.-F., Heithausen, A., Pérault, M., Stutzki, J., Puget, J.-L., Bensch, F. 1998, *A&A*, 331, 669
- Falgarone, E., Phillips, T.G. 1990, *ApJ*, 359, 344
- Falkovich, G., Lebedev, V. 1997, *Phys. Rev. Lett.*, 79, 4159
- Forster, D., Nelson, D.R., Stephen, M.J. 1977, *Phys. Rev. A*, 16, 732
- Franco, J., Carraminana, A. (eds.) 1999, *Interstellar Turbulence*, Cambridge University Press
- Frisch, U. 1995, *Turbulence – The Legacy of A. N. Kolmogorov*, Cambridge University Press
- Gammie, C.F., Ostriker, E. E.C. 1996, *ApJ*, 466, 814
- Hockney, R.W., Eastwood, J.W. 1988, *Computer Simulation using Particles*, IOP Publishing Ltd., Bristol and Philadelphia
- Jahyesh, Warhaft, Z. 1991, *Phys. Rev. Lett.*, 67, 3503
- Kleiner, S.C., Dickman, R.L. 1987, *ApJ*, 312, 837

- Klessen, R.S. 1997, MNRAS, 292, 11
- Klessen, R.S., Burkert, A., Bate, M.R. 1998, ApJ, 501, L205
- Klessen, R.S., Burkert, A. 2000, ApJS, 128 in press (astro-ph/9904090)
- Klessen, R.S., Heitsch, F., Mac Low, M.-M. 2000, ApJ, accepted (astro-ph/9911068)
- Kida, S., Murakami, Y. 1989, Fluid Dyn. Res., 4, 347
- Kitamura, Y., Sunada, K., Hayashi, M., Hasegawa, T. 1993, ApJ, 413, 221
- Kolmogorov, A.N. 1941, Dokl. Akad. Nauk SSSR, 30, 301 (reprinted in Proc. R. Soc. Lond. A, 434, 9 (1991))
- Lamballais, E., Lesieur, M., Métais, O. 1997, Phys. Rev. E, 56, 761
- LaRosa, T.N., Shore, S.N., Magnani, L. 1999, ApJ, 512, 761
- Lesieur, M. 1997, Turbulence in Fluids, 3. ed., Kluwer Academic Publishers, Dordrecht
- Lis, D.C., Keene, J., Phillips, T.G., Pety, J. 1998, ApJ, 504, 889
- Lis, D.C., Pety, J., Phillips, T.G., Falgarone, E. 1996, ApJ, 463, 623
- Machiels, L., Deville, M.O. 1998, J. Comp. Phys., 145, 256
- Mac Low, M.-M. 1999, ApJ, 524, 169
- Mac Low, M.-M., Klessen, R.S., Burkert, A., Smith, M.D. 1998, Phys. Rev. Lett., 80, 2754
- Mac Low, M.-M., Ossenkopf, V. 2000, A&A, 353, 339
- Miesch, M.S., Bally, J. 1994, ApJ, 429, 645
- Miesch, M.S., Scalo, J.M. 1995, ApJ, 450, L27
- Miesch, M.S., Scalo, J.M., Bally, J. 1998, ApJ, submitted (astro-ph/9810427)
- Monaghan, J.J. 1992, ARA&A, 30, 543
- Monaghan, J.J., Gingold, R.A. 1983, J. Comp. Phys., 52, 135
- Padoan, P., Nordlund, Å, Jones, B.J.T. 1997, MNRAS, 288, 145
- Padoan, P., Nordlund, Å. 1999, ApJ, 526, 279
- Passot, T., Vázquez-Semadeni, E. 1998, Phys. Rev. E, 58, 4501
- Porter, D.H., Pouquet, A., Woodward, P.R. 1994, Phys. Fluids, 6, 2133
- Scalo, J.M. 1984, ApJ, 7, 556
- Scalo, J.M., Vázquez-Semadeni, E., Chappell, D., Passot, T. 1998, ApJ, 504, 835
- She, Z.-S. 1991, Fluid Dyn. Res., 8, 143

- She, Z.-S., Jackson, E., Orszag, S.A. 1991, Proc. R. Soc. Lond. A, 434, 101
- Steinmetz, M. 1996, MNRAS, 278, 1005
- Stone, J. M., Ostriker, E. C., Gammie, C. F.: 1998, ApJ, 508, L99
- Stutzki, J., Güsten, R. 1990, ApJ, 412, 233
- Sugimoto, D., Chikada, Y., Makino, J., Ito, T., Ebisuzaki, T., Umemura, M. 1990, Nature, 345, 33
- Umemura, M., Fukushige, T., Makino, J., Ebisuzaki, T., Sugimoto, D., Turner, E.L., Loeb, A. 1993, PASJ, 45, 311
- Vainshtein, S.I. 1997, Phys. Rev. E, 56, 6787
- Van der Marel, R. P., Franx, M. 1993, ApJ, 407, 525
- Vázquez-Semadeni, E. 1994, ApJ, 423, 681
- Vázquez-Semadeni, E., Gazol, A. 1995, A&A, 303, 204
- Vincent, A., Meneguzzi, M. 1991, J. Fluid Mech., 225, 1
- Vio, R., Fasano, G., Lazzarin, M., Lessi, O. 1994, A&A, 289, 640
- Williams, J.P., De Geus, E.J., Blitz, L. 1994, ApJ, 428, 693
- Williams, J. P., Blitz, L., McKee, C. F. 2000, in Protostars and Planets IV, eds. V. Mannings, A. Boss & S. Russell, in press

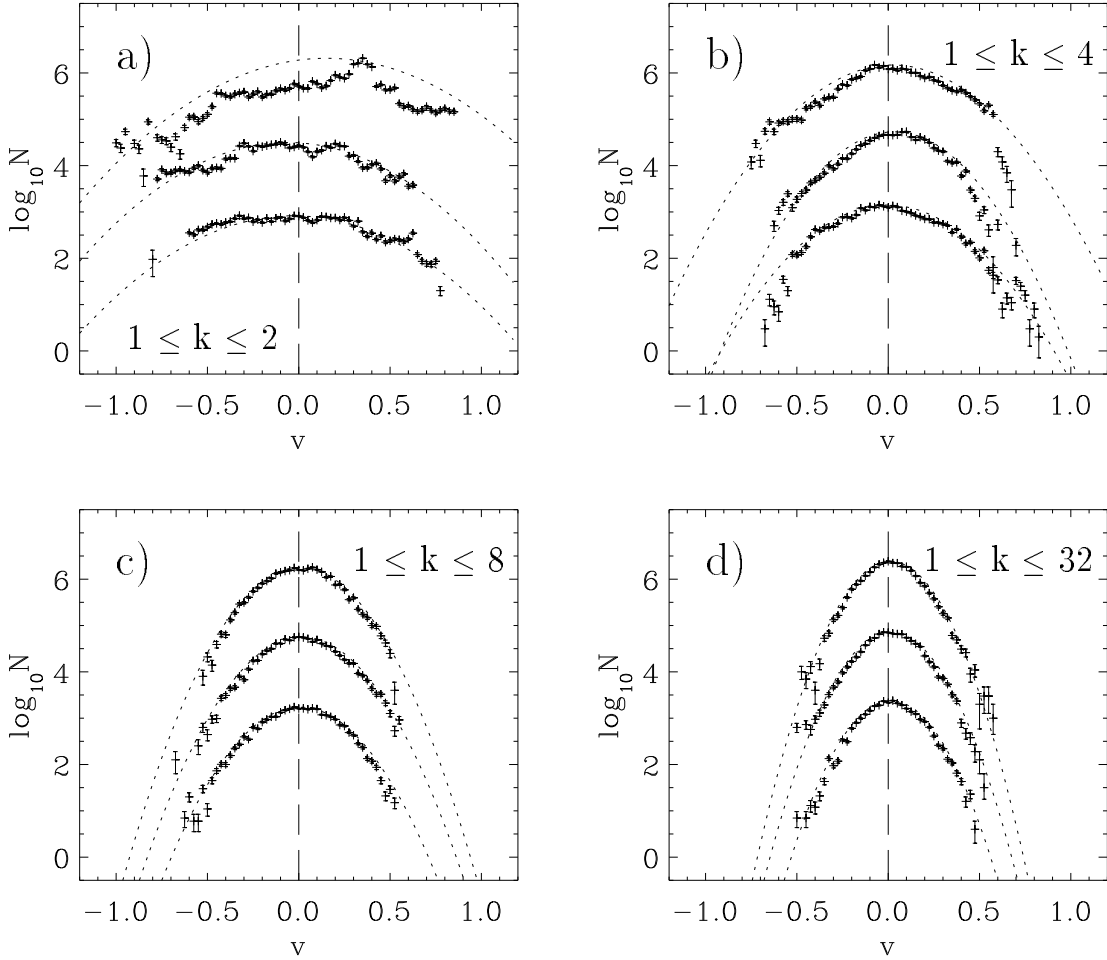


Fig. 1.— Pdf’s of line centroids for a homogeneous gaseous medium with Gaussian velocity field. The power spectrum is $P(k) = \text{const.}$ with wave numbers in the intervals (a) $1 \leq k \leq 2$, (b) $1 \leq k \leq 4$, (c) $1 \leq k \leq 8$, to (d) $1 \leq k \leq 32$. All other modes are suppressed. Each figure plots pdf’s of the x -, y -, and z -component of the velocity offset by $\Delta \log_{10} N = 1.5$ (lowest, middle, and upper distribution, respectively). The length of the error bars is determined by the square root of the numbers of entries per velocity bin. The Gaussian fit from the first two moments is shown with dotted lines.

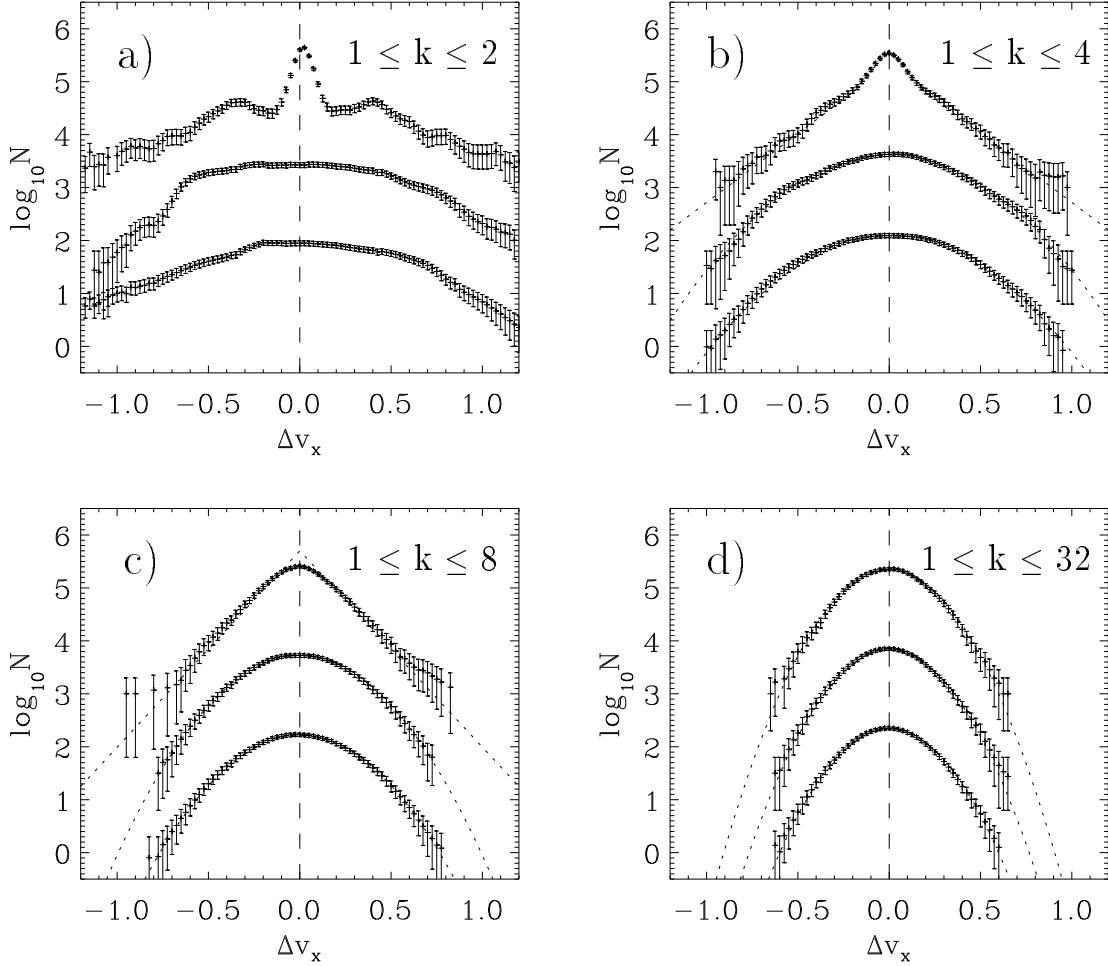


Fig. 2.— Pdf’s of line centroid increments for the same systems as in Fig. 1: (a) $1 \leq k \leq 2$, (b) $1 \leq k \leq 4$, (c) $1 \leq k \leq 8$, to (d) $1 \leq k \leq 32$. Each plot shows the distribution of centroid velocity differences between locations separated by the distance Δr — upper curve: $\Delta r = 1/32$, middle curve: $\Delta r = 10/32$, and lower curve: $\Delta r = 30/32$. Only the velocity component for the line-of-sight parallel to the x -axis is considered. Again, the dotted lines represent the best fit Gaussian, except for the upper curve in (b) and (c) where the best exponential fit is shown.

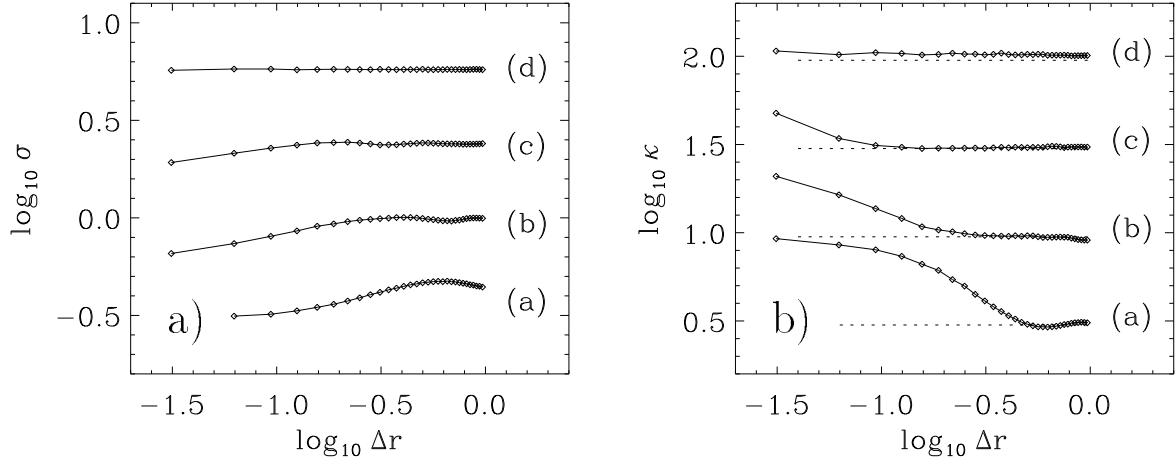


Fig. 3.— (a) The second, dispersion σ , and (b) the fourth moment, kurtosis κ , of the distribution of velocity increments displayed in Fig. 2 as function of spatial lag Δr . The letters on the right-hand side indicate correspondence to the previous figure. Each plot is offset by $\Delta \log_{10} \sigma = 0.5$ and $\Delta \log_{10} \kappa = 0.5$, and in (b) the horizontal dotted line indicates the value for a Gaussian $\kappa = 3$ ($\log_{10} \kappa = 0.48$).

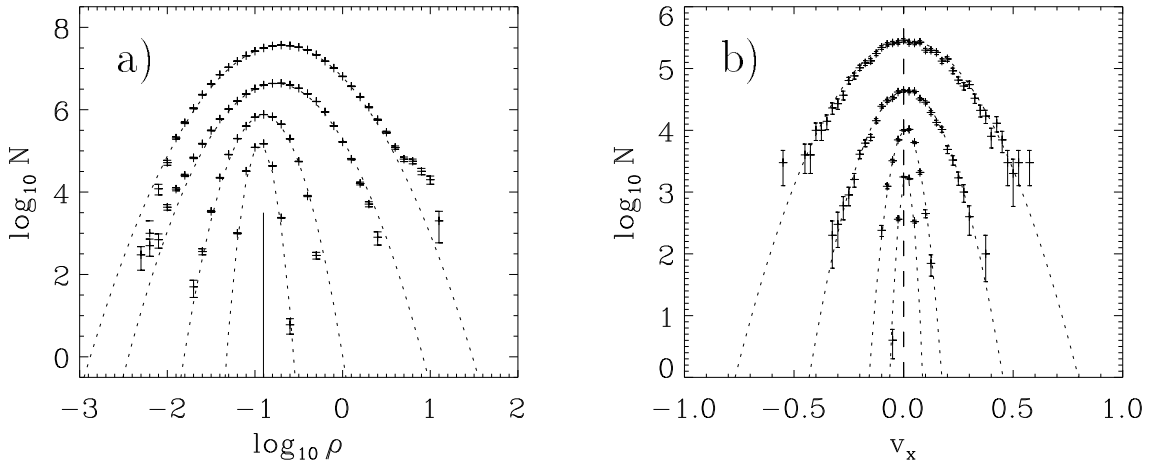


Fig. 4.— Pdf's of (a) density and of (b) centroid velocities for the line-of-sight being parallel to the x -axis of the system. The pdf's are obtained at four different phases of the dynamical evolution of the system (see the main text), at $t = 0.2$ (upper curves), at $t = 0.6$ (second curve from the top), at $t = 3.5$ (third curve), and at $t = 20.0$ (lowest curve). These times correspond to Mach numbers $M = 5.0$, $M = 2.5$, $M = 1.0$, and $M = 0.3$, respectively. For each distribution, the best-fit Gaussian is indicated using dotted lines.

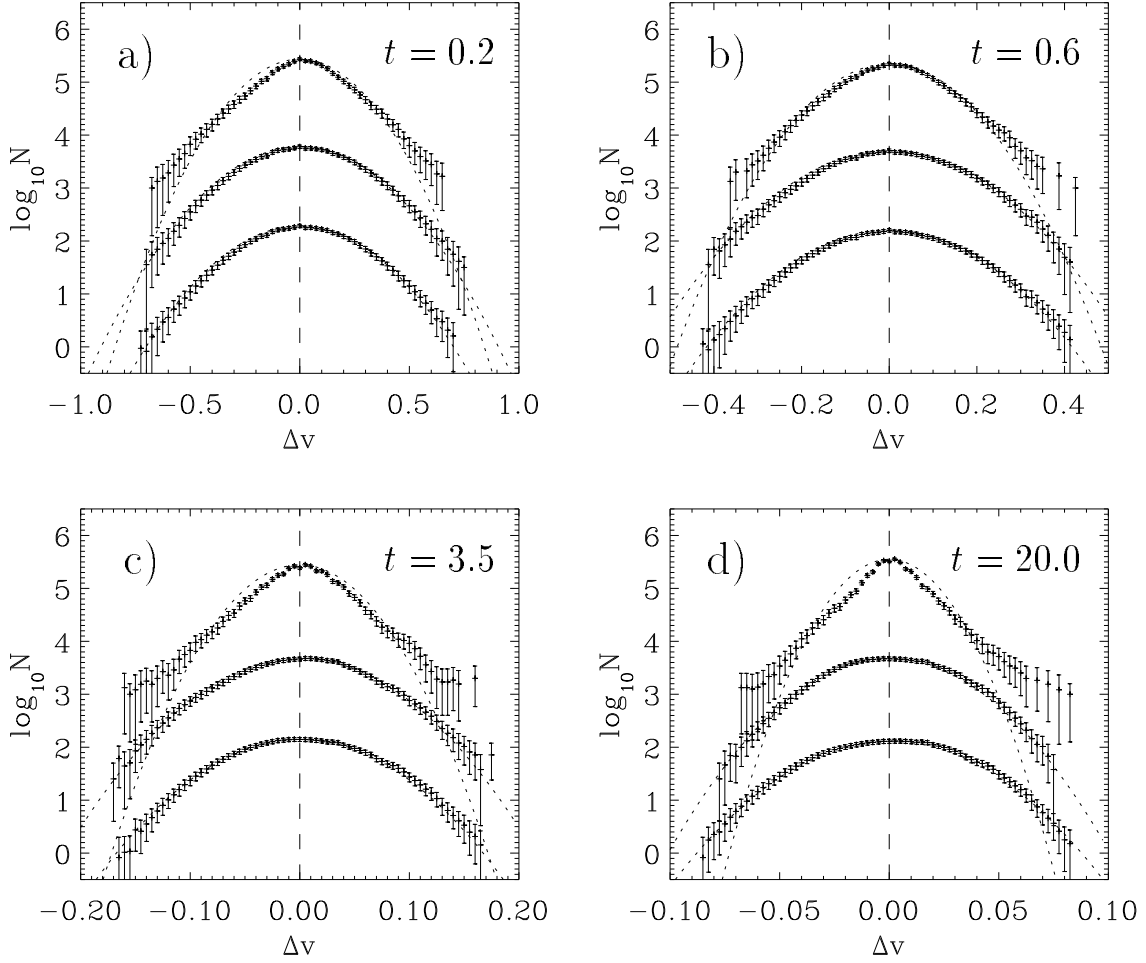


Fig. 5.— Pdf’s of the x -component of the centroid velocity increments for three spatial lags: upper curve – $\Delta r = 1/32$, middle curve – $\Delta r = 10/32$, and lower curve – $\Delta r = 30/32$. As in Fig. 4, the pdf’s are obtained at (a) $t = 0.2$, (b) $t = 0.6$, (c) $t = 3.5$, and (d) $t = 20.0$. The Gaussian fits are again indicated by dotted lines.

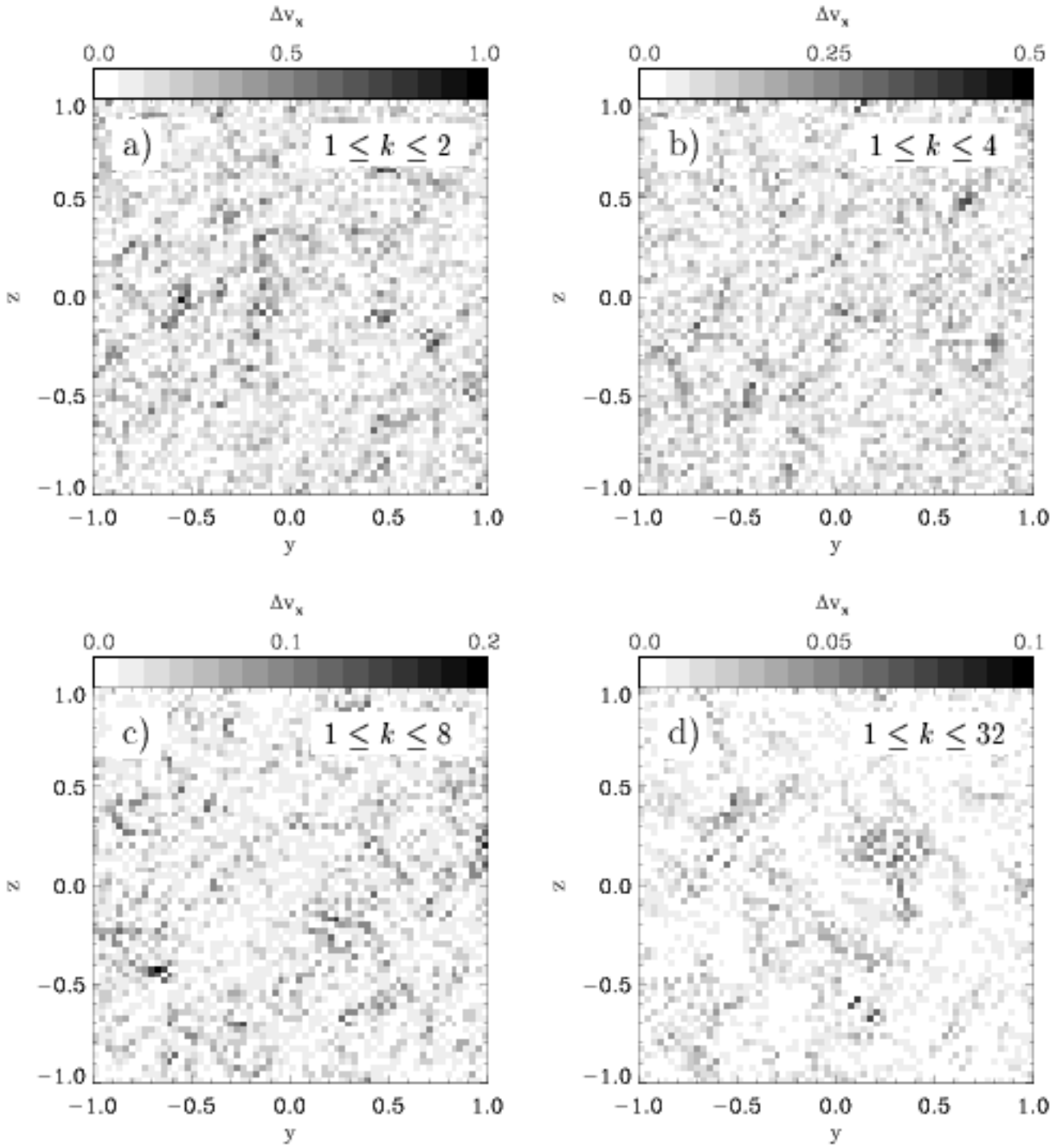


Fig. 6.— 2-dimensional distribution (in the yz -plane) of centroid increments for velocity profiles along the x -axis of the system between locations separated by a vector lag $\Delta\vec{r} = (1/32, 1/32)$. Analog to the previous figures, the data are displayed for times (a) $t = 0.2$, (b) $t = 0.6$, (c) $t = 3.5$, and (d) $t = 20.0$. The magnitude of the velocity increment Δv_x is indicated at the top of each plot; note the different scaling.

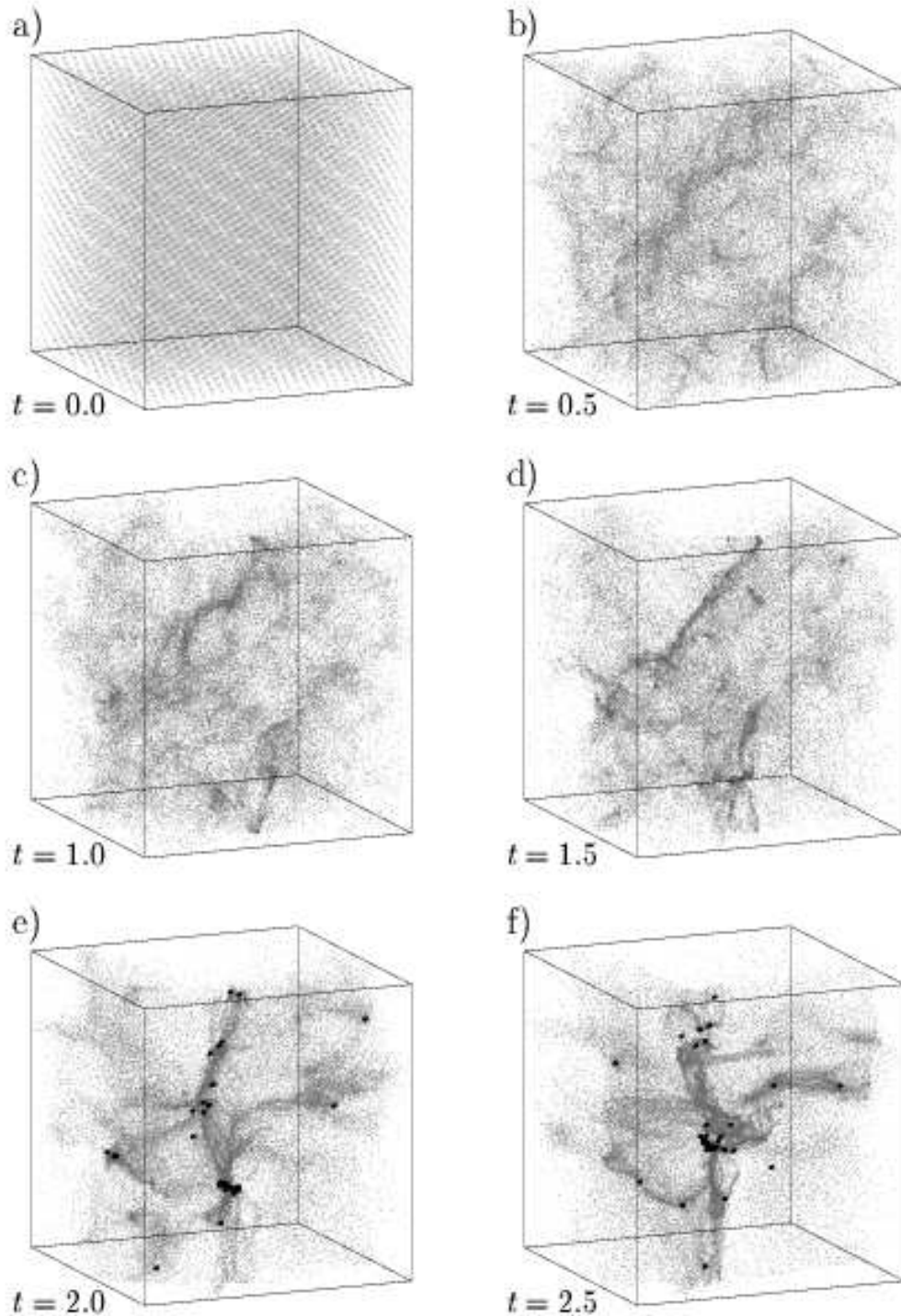


Fig. 7.— The 3-dimensional gas distribution in the SPH simulation of initially supersonic, decaying turbulence at six different stages of the dynamical evolution. Only every fourth of the 200 000 SPH particles is displayed. (a) The first plot shows the homogeneous initial density field. Further snapshots of the system are taken at (b) $t = 0.5$, (c) $t = 1.0$, (d) $t = 1.5$, (e) $t = 2.0$, and (f) $t = 2.5$, where time is measured in units of the free-fall time scale. The system evolves into a network of interacting shocks creating a filamentary density structure. As the turbulent flow decays, local collapse becomes possible. Dense cores (substituted by ‘sink’ particles) are indicated by dark dots. In (e) the mass accumulated in collapsed cores

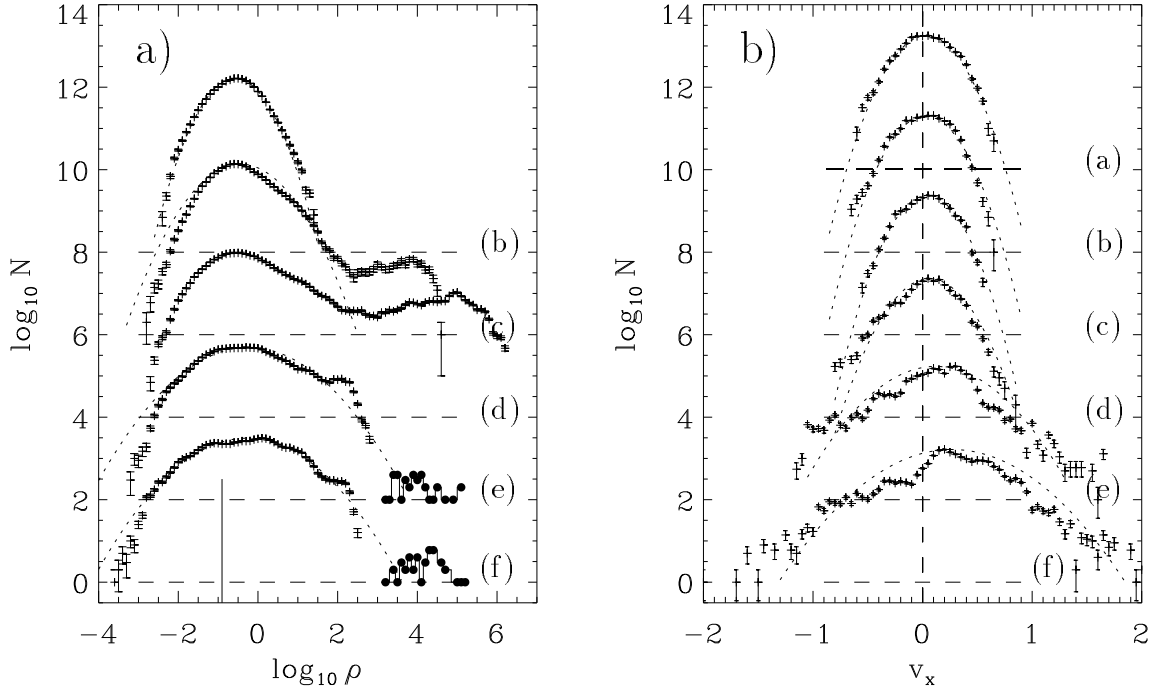


Fig. 8.— Pdf’s of (a) the density and (b) the x -component of line centroids for the simulation of initially supersonic, decaying turbulence in self-gravitating gas. The time sequence is the same as in the previous figure as denoted by the corresponding letter to the right of each pdf. In the left panel, the initial density is indicated by the vertical line at $\rho = 1/8$. The density contributions from collapsed cores forming in the late stages of the evolution are indicated by solid dots. The core density corresponds to a mean value computed from the core mass divided by its accretion volume. In both figures, each pdf is offset by $\Delta \log_{10} N = 2.0$ with the base $\log_{10} N = 0.0$ indicated by horizontal dashed lines. The best-fit Gaussian curves are shown as dotted lines.

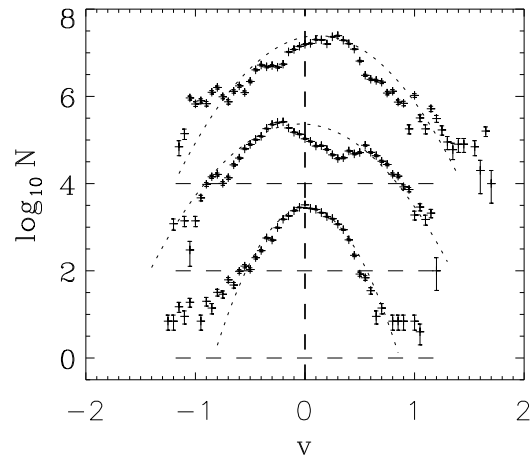


Fig. 9.— Centroid velocity pdf's for the simulation of initially supersonic, decaying turbulence in self-gravitating gas at $t = 2.0$ for the line-of-sight being along the x -axis (upper curve – it is identical to the fifth pdf in Fig. 8b), along the y -axis (middle), and along the z -axis of the system (bottom). Each distribution is offset by $\Delta \log_{10} N = 2.0$ with the horizontal lines indicating the base $\log_{10} N = 0.0$. The pdf's of various projections and velocity components can differ considerably.

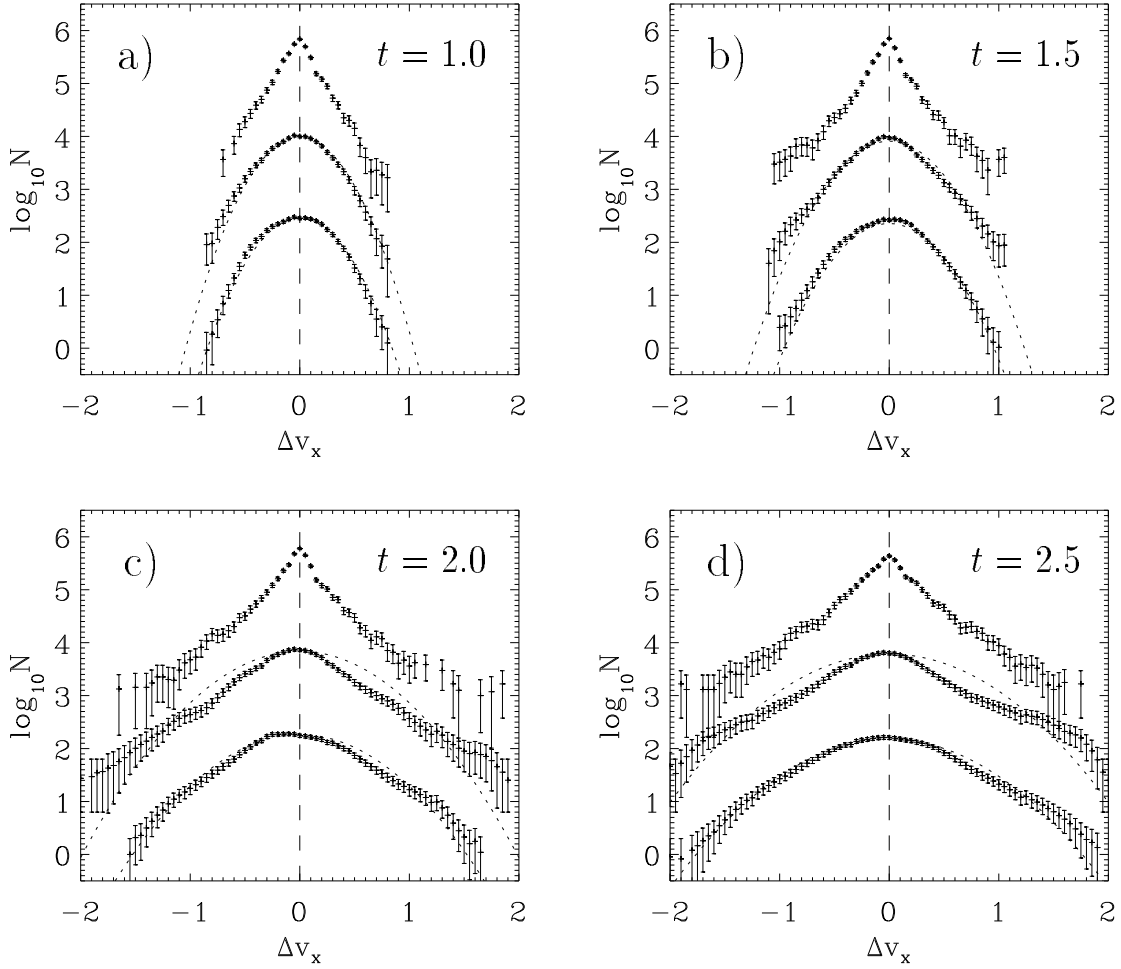


Fig. 10.— Pdf’s of the x -component of the centroid velocity increments for three spatial lags: upper curve – $\Delta r = 1/32$, middle curve – $\Delta r = 10/32$, and lower curve – $\Delta r = 30/32$. The functions are computed from the simulation of initially supersonic, decaying turbulence in self-gravitating gas at (a) $t = 1.0$, (b) $t = 1.5$, (c) $t = 2.0$, and (d) $t = 2.5$. Where appropriate, the Gaussian curves obtained from the first two moments of the distribution are indicated by dotted lines. During the early phases of the evolution, the flow is similar to pure hydrodynamic turbulence (the pdf’s are close to the ones in Fig. 5). As turbulent energy decays self-gravity gains influence and the late stages of the evolution are dominated by gravitational contraction. Consequently the pdf’s in the sequence (a) to (d) become more and more non-Gaussian with the progression of time. This concerns the pdf’s for small to intermediate lags Δr .

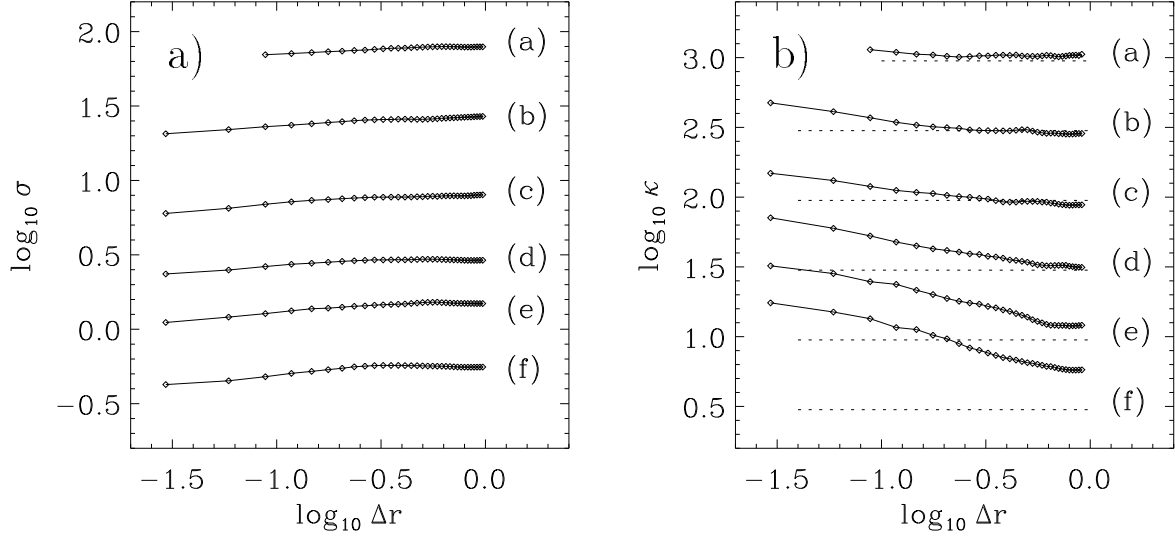


Fig. 11.— (a) The second, dispersion σ , and (b) the fourth moment, kurtosis κ , as function of spatial lag Δr for the distribution of velocity increments in the simulation of self-gravitating, decaying, supersonic turbulence. The letters on the right-hand side indicate the time at which the increment pdf's are computed ranging from $t = 0.0$ at the top down to $t = 2.5$ at the bottom (see Fig.'s 7 or 8). Each pdf is offset by $\Delta \log_{10} \sigma = 0.5$ and $\Delta \log_{10} \kappa = 0.5$, respectively.

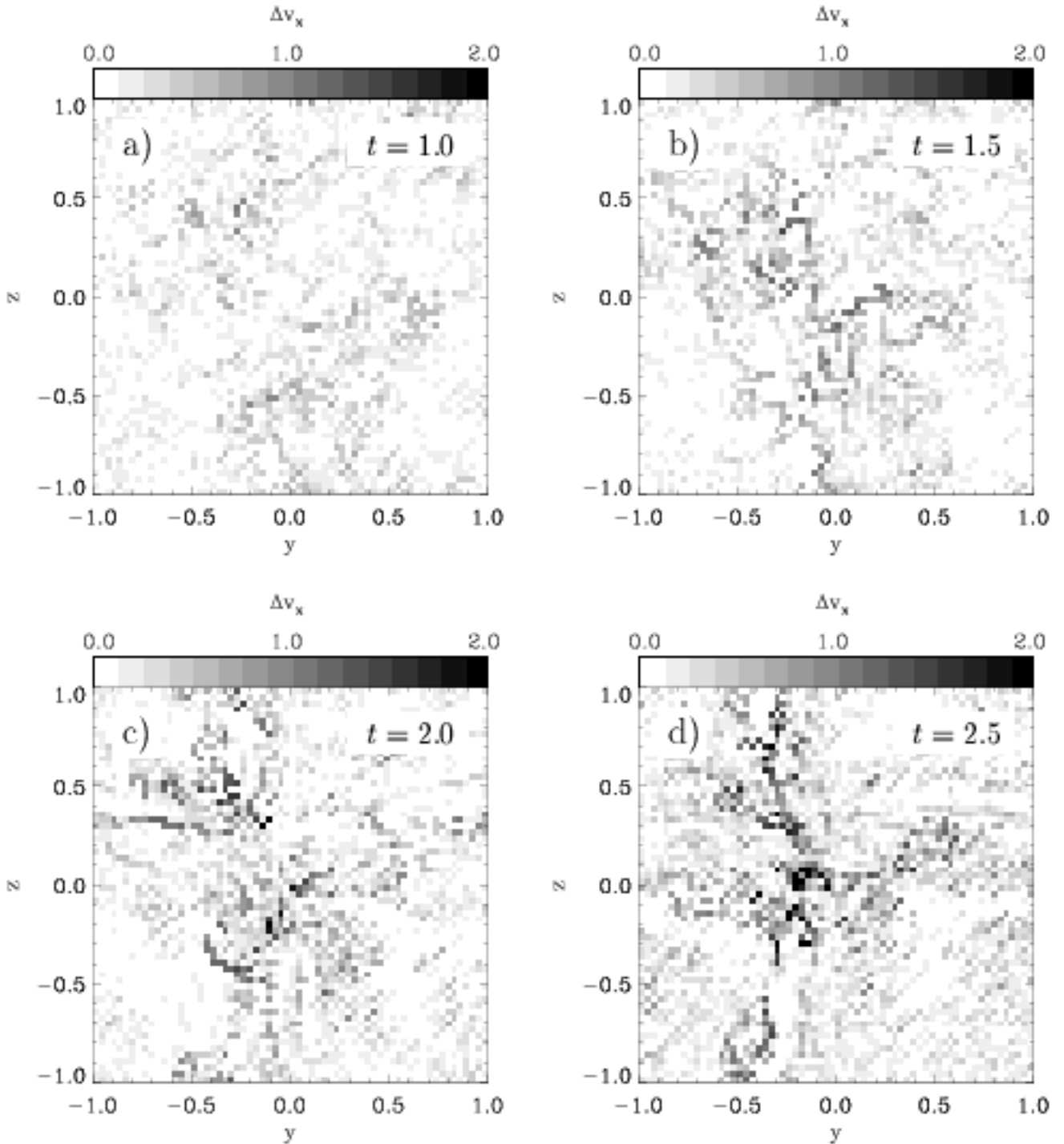


Fig. 12.— 2-dimensional distribution (in the yz -plane) of centroid increments for velocity profiles along the x -axis of the system between locations separated by a vector lag $\Delta\vec{r} = (1/32, 1/32)$ for the simulation of self-gravitating, decaying, supersonic turbulence. Analog to Fig. 10, the data are displayed for times (a) $t = 1.0$, (b) $t = 1.5$, (c) $t = 2.0$, and (d) $t = 2.5$. The magnitude of the velocity increment Δv_x is indicated at the top of each plot.

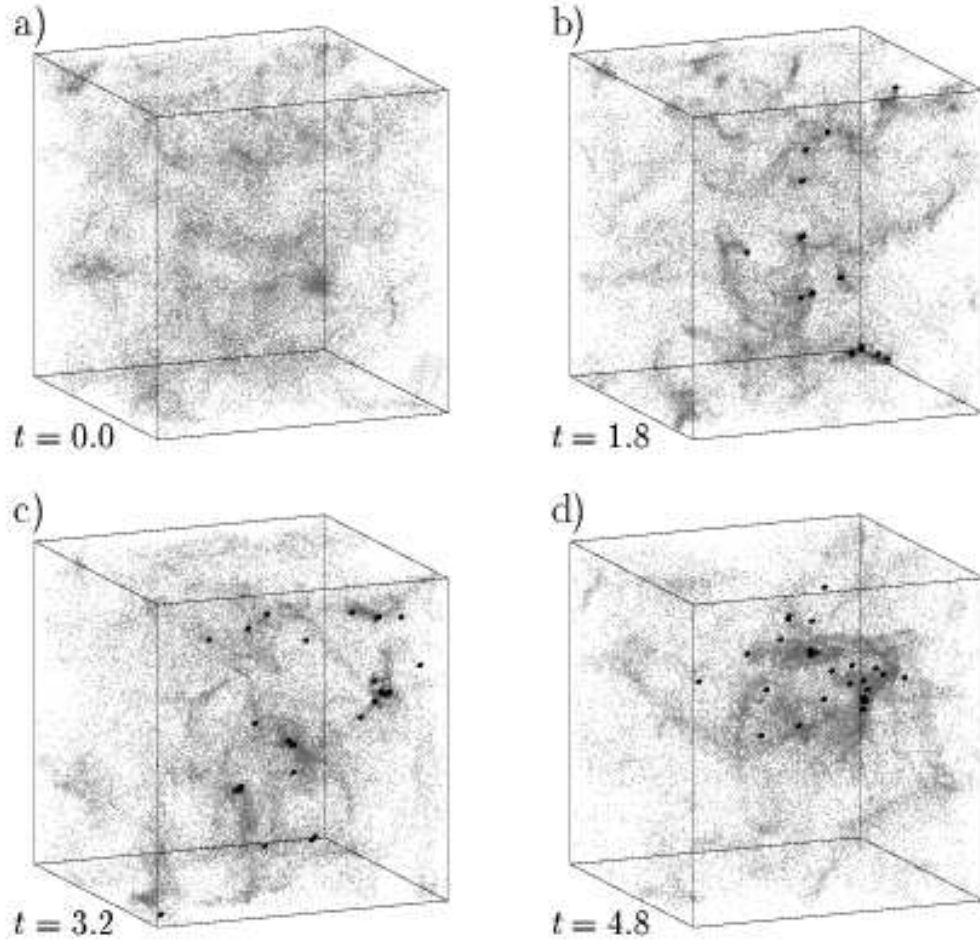


Fig. 13.— The 3-dimensional gas distribution in the simulation of constantly driven turbulence in self-gravitating gas. Once the turbulent kinetic energy reaches the equilibrium level, gravity is turned on. This stage is displayed in (a). The next three snapshots of the system are taken at times (b) $t = 1.8$, when 20% of the gas mass is in dense collapsed cores (as indicated by black dots – cf. with Fig. 7), at (c) $t = 3.2$, when the mass in cores is 40% of the total mass, and at (d) $t = 4.8$, when the cluster of cores contains 60% of the system mass. Time is given in units of the free-fall time, but unlike in the previous cases it is counted from the point gravity is turned on.

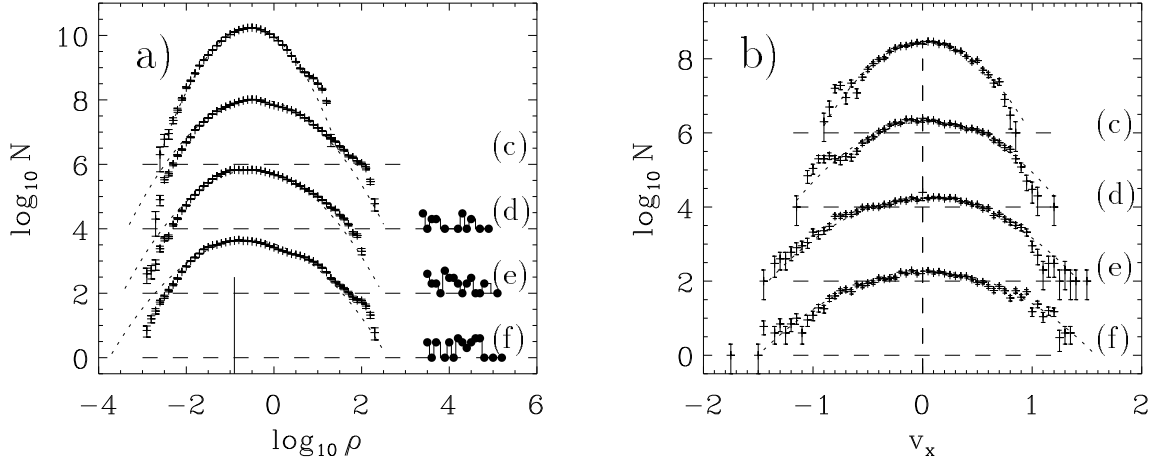


Fig. 14.— Pdf's of (a) the density and (b) the x -component of line centroids for the simulation of driven turbulence in self-gravitating gas. The time sequence is the same as in the previous figure as indicated by the letters to the right. Each pdf is offset by $\Delta \log_{10} N = 2.0$ with the base $\log_{10} N = 0.0$ indicated by horizontal dashed lines. The best-fit Gaussian curves are shown as dotted lines. The density contributions in (a) coming from collapsed cores are indicated by solid dots.

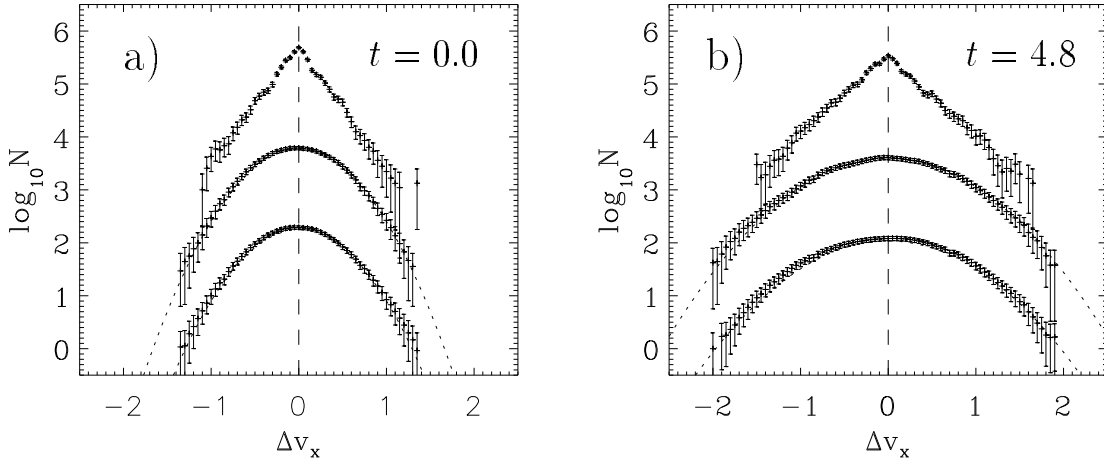


Fig. 15.— Pdf's of the x -component of the centroid velocity increments for three spatial lags: upper curve – $\Delta r = 1/32$, middle curve – $\Delta r = 10/32$, and lower curve – $\Delta r = 30/32$. The functions are computed from the simulation of driven, self-gravitating, supersonic turbulence at (a) $t = 0.0$ and (b) $t = 4.8$. As in the previous models the increment pdf's for small spatial lags are approximately exponential, however, the pdf's for larger separations remain close to Gaussian throughout the evolution.

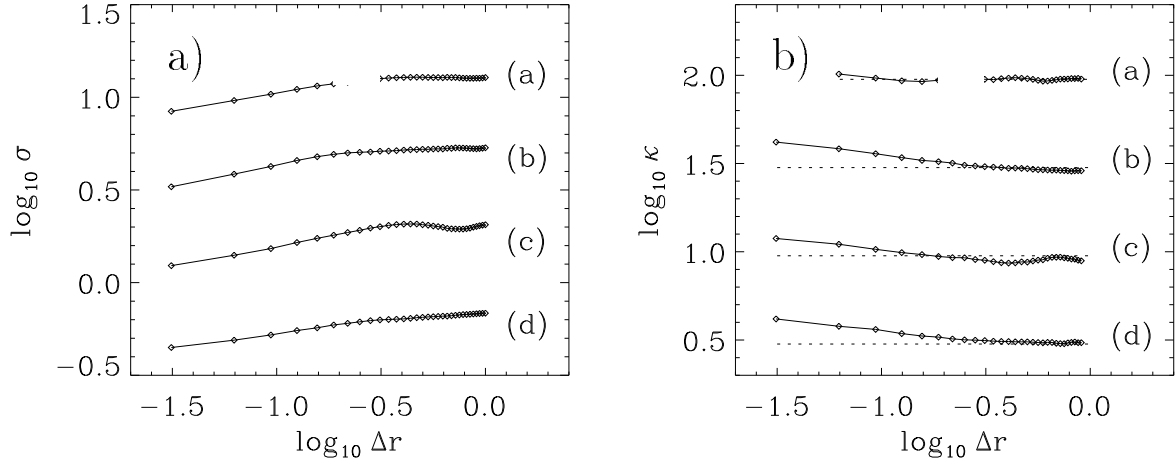


Fig. 16.— (a) The second, dispersion σ , and (b) the fourth moment, kurtosis κ , as function of spatial lag Δr for the distribution of velocity increments in the simulation of driven, self-gravitating, supersonic turbulence. The letters on the right-hand side indicate again the correspondence to the times in Fig. 13. Each pdf is offset by $\Delta \log_{10} \sigma = 0.5$ and $\Delta \log_{10} \kappa = 0.5$, respectively.

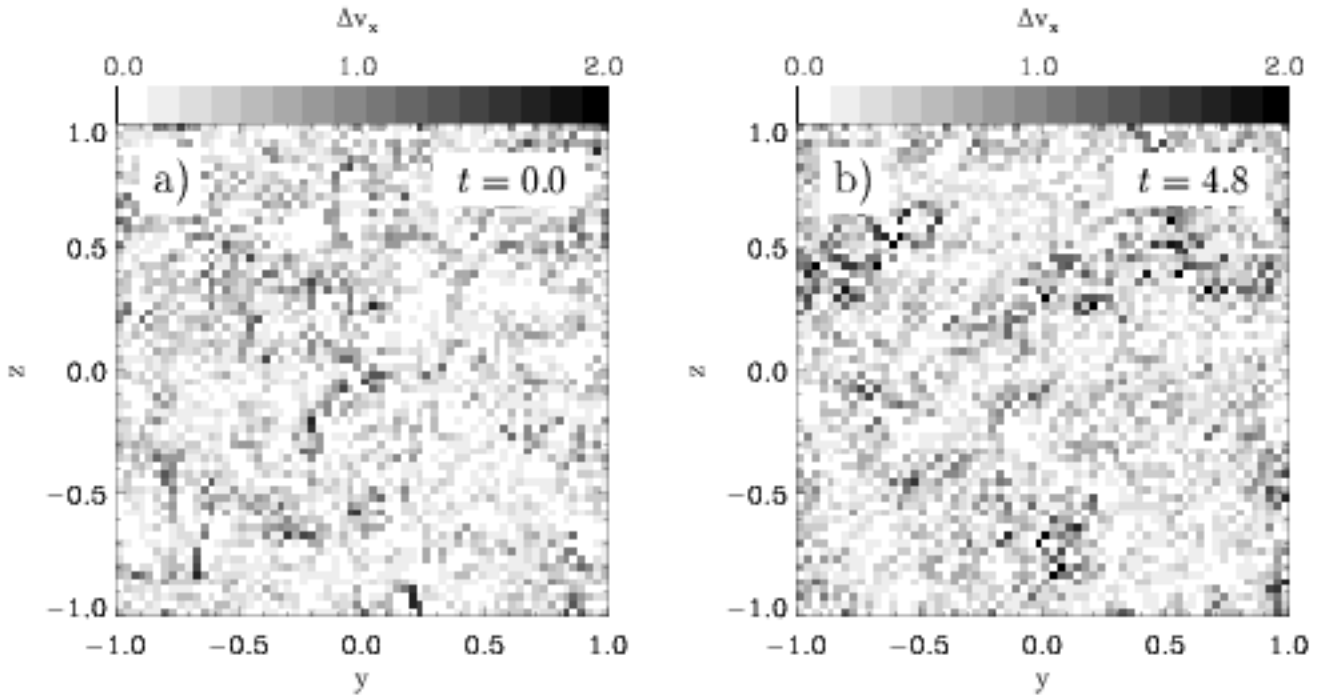


Fig. 17.— 2-dimensional distribution (in the yz -plane) of the absolute value of the x -component of centroid velocity increments between locations separated by a vector lag $\Delta\vec{r} = (1/32, 1/32)$ for the simulation of driven self-gravitating supersonic turbulence. The data are displayed at times (a) $t = 0.0$, and (b) $t = 4.8$. The scaling is indicated at the top of each figure.